

Characterizing differences in intraocular pressure and biomechanical parameters between two generations of dynamic bidirectional air-puff tonometers in subjects with central and peripheral keratoconus and in healthy controls

Thesis

Presented in Partial Fulfillment of the Requirements for the Degree Master of Science in the Graduate School of The Ohio State University

By

Maddison M. Fortman, B.S.

Graduate Program in Vision Science

The Ohio State University

2024

Thesis Committee

Dr. Phillip Yuhas, Co-Advisor

Dr. Cynthia Roberts, Co-Advisor

Dr. Heather Anderson, Committee Member

Dr. Nicky Lai, Committee Member

Copyrighted by
Maddison M. Fortman
2024

Abstract

Changes to the air jet delivery and applanation detection systems in the newest generation Ocular Response Analyzer (G3 ORA) altered the morphology of its output waveforms, compared to the original device (G1 ORA). These waveforms represent both the corneal deformation response to an air puff and temporal pressure profile of the air puff itself. It is known that keratoconus alters the corneal deformation response, causing the ORA waveforms to vary substantially between normal and keratoconic eyes. The Keratoconus Match Index (KMI) of the G1 ORA uses waveform parameters to differentiate keratoconic eyes from normal eyes, but it was not adapted for the updated G3 ORA. It is unknown whether the original KMI is effective in identifying keratoconic eyes when using the G3 ORA, leaving a gap in our ability to use a biomechanical approach to supplement our ability to detect early keratoconus. **Therefore, the initial aims of this study were 1) to quantify differences in intraocular-pressure metrics and biomechanical waveform parameters, both between two versions of the device and between subjects with keratoconus and controls; and 2) to evaluate the performance of the original KMI in identifying keratoconic eyes when applied to G3 ORA measurement data.** Furthermore, keratoconus is characterized by focal weakness in the area of cone formation, surrounded by stronger tissue. Cone location impact on biomechanics of the cornea has never been tested using the ORA. Therefore, **the third**

purpose of this study is to investigate whether cone location influences the ORA-measured biomechanical waveform parameters of the cornea in keratoconus.

Fifty ($n = 50$) subjects diagnosed with keratoconus (mean \pm standard deviation age = 38 ± 13 years; 28% female; 58% White) and 144 ($n = 144$) healthy control subjects (age = 39 ± 17 years; 61% female; 81% White) were prospectively recruited. Corneal compensated IOP (IOP_{cc}), Goldmann-correlated IOP (IOP_g), and waveform parameters including corneal hysteresis (CH), waveform score (WS), area under first applanation peak (p1area), area under second applanation peak (p2area), height of first applanation peak (h1), height of second applanation peak (h2), width of first applanation peak (w1), width of second applanation peak (w2), and Keratoconus Match Index (KMI), were collected in both eyes with the G1 ORA and with the G3 ORA. Four measurements were taken on each eye, and the measurement with the highest waveform score was analyzed. Paired t-tests were used to compare results between the two generations of ORAs, and t-tests were used to compare results between the cohorts ($\alpha = 0.002$). Receiver operating characteristic (ROC) Areas Under the Curve (AUC) were evaluated to compare the diagnostic performances of KMI in differentiating keratoconic eyes from normal eyes when using the G1 ORA and the G3 ORA.

Only the keratoconic eyes were considered in the cone-location aspect of the study. Medmont corneal topography was conducted on both eyes, and axial and tangential curvature were analyzed using custom software. Cones in the central 3 mm of the cornea were considered central, and cones outside the central 3 mm were considered peripheral. T-tests compared differences in waveform parameters between cohorts. Significance threshold was $\alpha = 0.05$ for all analyses.

Seventy-eight were analyzed in the case cohort, and 144 eyes were analyzed in the control cohort. In the case cohort, the G3 ORA measured significantly greater CH (inter-device difference = 0.499 ± 1.24 mmHg), WS (0.97 ± 1.68), p1area (648 ± 726), p2area (1865 ± 1230), h1 (92.0 ± 97.6), h2 (88.3 ± 84.4), w2 (6.32 ± 6.38), and KMI (0.682 ± 0.404), compared to the G1 ORA. The G1 ORA measured significantly greater w1 (4.54 ± 4.34) than the G3 ORA in the case cohort. In the control cohort, the G3 ORA measured significantly greater CH (0.497 ± 1.13 mmHg), WS (0.567 ± 1.35), p1area (479 ± 837), p2area (3052 ± 1160), h1 (67.0 ± 83.7), h2 (128 ± 91.2), w2 (6.95 ± 4.14), and KMI (0.912 ± 0.323) than the G1 ORA. The G1 ORA measured significantly greater w1 (3.10 ± 2.66) than the G3 ORA. There were no statistically significant differences in IOPcc and IOPg between the two devices in either cohort.

When measured by the G1 ORA, the control cohort had significantly greater IOPcc (inter-cohort difference = 1.95 ± 3.15 mmHg), IOPg (4.94 ± 3.30 mmHg), CH (2.12 ± 1.80 mmHg), WS (1.88 ± 1.68), p1area (1654 ± 1140), p2area (1135 ± 907), h1 (139 ± 94.2), h2 (98.3 ± 92.9), and KMI (0.600 ± 0.384) than the case cohort. There were no statistically significant differences in w1 and w2 between the two cohorts. When measured by the G3 ORA, the control cohort had significantly greater IOPcc (1.74 ± 2.93 mmHg), IOPg (4.70 ± 3.37 mmHg), CH (2.13 ± 1.48 mmHg), WS (1.48 ± 1.41), p1area (1485 ± 1170), p2area (2332 ± 1370), h1 (114 ± 111), h2 (138 ± 101), w1 (1.38 ± 2.16), and KMI (0.830 ± 0.474) than the case cohort. The only parameter that did not significantly differ between the two cohorts was w2.

ROC AUC was marginally greater when KMI was used to differentiate keratoconic eyes from normal eyes with the G3 ORA (0.88) compared to the AUC when KMI was used with the G1 ORA (0.86).

The 78 eyes with keratoconus were analyzed further for the effect of cone location. According to the axial topography maps, 37 eyes had central cones and 41 eyes had peripheral cones. According to the tangential topography maps, 53 eyes had central cones, and 25 eyes had peripheral cones. For the axial-topography algorithm, WS was significantly higher in peripheral cones than central cones (inter-cohort difference = 1.27 ± 1.87). Peripheral cones had a significantly higher p1area (1047 ± 1346), p2area (1130 ± 1478), h1 (102 ± 147), and h2 (102 ± 127), than central cones. CH, w1, and w2, did not significantly differ between cohorts. There were similar results for the tangential topography algorithm, with a significant difference between the cohorts for p1area (855 ± 1389), p2area (860 ± 1531), h1 (81.7 ± 151), and h2 (92.1 ± 131).

These results suggest that the air jet delivery and applanation detection system changes incorporated in the G3 ORA did alter its quantification of biomechanical waveform parameters, compared to the G1 ORA. IOP outcomes were less effected. Therefore, caution must be taken when comparing results between the two generations of ORAs in clinic and in research studies. Additionally, this study agreed with previous studies that normal eyes are stiffer and produce higher IOP values than keratoconic eyes. The KMI originally developed for the G1 ORA performed similarly when used with input data from either G1 ORA or G3 ORA. The next step in this research is to optimize the Keratoconus Match Index metric for the G3 model.

This study also demonstrated that cone location affects the biomechanical response parameters measured under central loading of the cornea. The ORA delivers its air puff to the central cornea, so the fact that h_1 and h_2 and that p_1 area and p_2 area were smaller in the central cone cohort than in the peripheral cone cohort suggests that corneas with central cones are softer or more compliant centrally than corneas with peripheral cones, which is consistent with the location of the pathology. This result is additional evidence that corneal weakening in keratoconus is focal in nature and is consistent with localized disruption of lamellar orientation.

Acknowledgments

I am deeply grateful to my advisors, Dr. Phillip Yuhás and Dr. Cynthia Roberts, for their time, support and expertise throughout this study. Their mentorship is invaluable, and I am very fortunate to have trained under their guidance. I thank Dr. Roberts for sharing her wealth of knowledge; our conversations have expanded my abilities to critically analyze research and improve my writing. I also thank Dr. Yuhás for his advice throughout my time in this program, and for pushing me to reach my full potential as a student and researcher. I am also grateful to Michael Nye for his assistance in recruiting study participants. Lastly, I extend thanks to my fellow M.S. classmates for their camaraderie and encouragement throughout this program.

Vita

Education

2020B.S. Biology, Bowling Green State University

Publications

Fortman, M. M., Mahmoud, A. M., Roberts, C. J., & Yuhas, P. T. (2023). Intraocular pressure and biomechanical parameters measured with two generations of dynamic bidirectional air-puff tonometers in subjects with keratoconus and in healthy controls. *Invest. Ophthalmol Vis. Sci*, 64(8), 1701.

Yuhas, P. T., Fortman, M. M., Mahmoud, A. M., & Roberts, C. J. (2024). Keratoconus cone location influences ocular biomechanical parameters measured by the Ocular Response Analyzer. *Eye Vis (Lond)*, 11(1), 2. <https://doi.org/10.1186/s40662-023-00371-0>

Yuhas P. T., Fortman, M. M., Nye, M., Mahmoud, A. M., & Roberts, C. J. (2024). Waveform score influences the outcome metrics of the Ocular Response Analyzer in patients with keratoconus and in healthy controls. *Current Eye Research*. (under review)

Fields of Study

Major Field: Vision Science

Table of Contents

Abstract.....	ii
Acknowledgments	viii
Vita	viii
List of Tables.....	xi
List of Figures	xiii
Chapter 1. Introduction.....	1
Keratoconus.....	1
Management of Keratoconus	4
Diagnosis and Assessment of Keratoconus	6
Corneal Biomechanics	9
Ocular Response Analyzer.....	10
Biomechanical Parameters.....	12
Keratoconus Match Index	13
Cone Location	16
Chapter 2. Methods	18
Subject Recruitment and Inclusion Criteria.....	18
Data Collection.....	18
Inter-device Differences	19
Cone Location	21
Chapter 3. Results.....	24
Inter-device and Inter-cohort Differences with G1 ORA and G3 ORA	24
Ability of KMI to Differentiate Between Cases and Controls with G1 and G3 ORA...28	
Cone Location	29
Chapter 4. Discussion	37
Differences in IOP and Biomechanical Parameters Between G1 ORA and G3 ORA in Case and Control Cohorts	37

Differences in IOP and Biomechanical Parameters Between Case and Control Cohorts as Measured by G1 ORA and G3 ORA	41
Ability of KMI to Differentiate Between Cases and Controls with G1 ORA and G3 ORA	43
Cone Location	45
ORA Agreement with Past Evidence of Cone Location Impact on Biomechanical Parameters	49
Utilization of the ORA in Research and Clinic	50
Influence of Topography Algorithm.....	51
Study Limitations	52
Conclusions.....	53
References.....	55
Appendix A. Measurement-type Agreement for IOP and Biomechanical Parameters in the Case Cohort and Control Cohort.....	62

List of Tables

Table 1. Describes several of the 37 waveform parameters derived from an ORA waveform that are more commonly reported in the literature.	15
Table 2. Demographic characteristics of case and control participants. Values are mean \pm SD, unless otherwise noted.....	24
Table 3. Differences in corneal-compensated IOP (IOPcc), Goldmann-correlated IOP (IOPg), corneal hysteresis (CH), waveform score (WS), area under first applanation peak (p1area), area under second applanation peak (p2area), height of first applanation peak (h1), height of second applanation peak (h2), width of first applanation peak (w1), width of second applanation peak (w2), and Keratoconus Match Index (KMI) as measured by the G1 Ocular Response Analyzer (ORA) and the G3 ORA in the case cohort. *p<0.002, t-test. Values are mean \pm SD.....	26
Table 4. Differences in corneal-compensated IOP (IOPcc), Goldmann-correlated IOP (IOPg), corneal hysteresis (CH), waveform score (WS), area under first applanation peak (p1area), area under second applanation peak (p2area), height of first applanation peak (h1), height of second applanation peak (h2), width of first applanation peak (w1), width of second applanation peak (w2), and Keratoconus Match Index (KMI) as measured by the G1 Ocular Response Analyzer (ORA) and the G3 ORA in the control cohort. *p<0.002, t-test. Values are mean \pm SD.....	26
Table 5. Inter-cohort differences in corneal-compensated IOP (IOPcc), Goldmann-correlated IOP (IOPg), corneal hysteresis (CH), waveform score (WS), area under first applanation peak (p1area), area under second applanation peak (p2area), height of first applanation peak (h1), height of second applanation peak (h2), width of first applanation peak (w1), width of second applanation peak (w2), and Keratoconus Match Index (KMI), as measured by the G1 Ocular Response Analyzer. *p < 0.002, t-test. Values are mean \pm SD.....	27
Table 6. Inter-cohort differences in corneal-compensated IOP (IOPcc), Goldmann-correlated IOP (IOPg), corneal hysteresis (CH), waveform score (WS), area under first applanation peak (p1area), area under second applanation peak (p2area), height of first applanation peak (h1), height of second applanation peak (h2), width of first applanation peak (w1), width of second applanation peak (w2), and Keratoconus Match Index (KMI), as measured by the G3 Ocular Response Analyzer. *p < 0.002, t-test. Values are mean \pm SD.....	28
Table 7. Differences in keratometry from axial topography and maximum tangential curvature, as defined by Cspot magnitude, between central cones and peripheral cones. Table from Yuhas et al. 2024.....	31
Table 8. Differences in biomechanical parameters between central cones and peripheral cones for axial topography. Table from Yuhas et al. 2024.....	32

Table 9. Differences in biomechanical parameters between central cones and peripheral cones for tangential topography. Table from Yuhas et al. 2024.34

List of Figures

Figure 1. Generation of the ORA Waveform. a) Visual representation of the electro-optical detection system of the ORA 1) before appplanation 2) at first inward appplanation 3) at concavity b) A typical infrared (IR) signal (red) and the pressure signal (green) versus time 1) before appplanation 2) at first inward appplanation 3) at concavity. The absolute value of the IR signal is shown since both convex (positive) and concave (negative) corneal curvatures disperse the incident IR light similarly. Figure modified from Luce and Taylor, 2016.....	11
Figure 2. Sample G1 ORA waveforms from (A) a control subject and (B) a case subject. The y-axis is number of photons aligned with the detector of the device, and the x-axis is time (ms). The green trace is air pressure created by the piston of the device. The red trace is the number of photons reaching the detector. Figure from Fortman et al. 2023...	15
Figure 3. Example waveform parameters. (a) Area of the first peak (p1area) and area of the second peak (p2area), (b) width of the first peak (w1) and width of the second peak (w2), and (c) height of the first peak (h1) and height of the second peak (h2) parameters identified on a representative pressure-applanation waveform generated by the Ocular Response Analyzer. The green traces represent the air pressure delivered to the cornea. The red traces represent the number of photons reflected off the corneal surface and into the infrared light sensor. Peak 1 occurs during first corneal appplanation, which happens during inward deformation; and Peak 2 occurs during second corneal appplanation, which happens during the outward recovery after cessation of the air puff. The waveform parameters are indicated in purple. The dark blue solid boxes mark the location along the pressure curve where the peaks of the infrared waveform occur. WS is waveform score. From Yuhas et al., 2024.....	20
Figure 4. Receiver-operator characteristic (ROC) curves for (A) keratoconus match index (KMI) with the G1 Ocular Response Analyzer (ORA), (B) KMI with the G3 ORA.....	29
Figure 5. Cone location by cohort. Location of the cone for 78 eyes with keratoconus (a) for axial-topography and (b) for tangential-topography. Central cones (light blue) were defined as being within a 1.5 mm radius from the center of the cornea, and peripheral cones (light red) were defined as being outside of a 1.5 mm radius from the center of the cornea. The dark blue line represents the normal distribution curve. Figure from Yuhas et al. 2024.	30
Figure 6. Associations between cone location according to axial topography and biomechanical parameters. Scatter plots showing the relationships between cone location and (a) wave score, (b) area of the second peak (p2area), (c) height of the second peak (h2), (d) area of the first peak (p1area), (e) height of the first peak (h1), (f) width of the first peak (w1), (g) width of the second peak (w2), and (h) corneal hysteresis (CH).	

Linear regression lines are solid gray. N=78 eyes with keratoconus. Figure from Yuhas et al. 2024.....35

Figure 7. Associations between cone location according to tangential topography and biomechanical parameters. Scatter plots showing the relationships between cone location and (a) area of the second peak (p2area), (b) height of the first peak (h1), (c) height of the second peak (h2), (d) wave score, (e) area of the first peak (p1area), (f) width of the first peak (w1), (g) width of the second peak (w2), and (h) corneal hysteresis (CH). Linear regression lines are solid gray. N=78 eyes with keratoconus. Figure from Yuhas et al. 2024.....36

Figure 8. Schematic representation of the effect that corneal stiffness has on reflected photons. A stiff central cornea (a) results in a broader area of applanation, and thus more photons reflected into the photodetector of the ORA, than a compliant central cornea (b), such as with a central cone, which has a narrow area of applanation.....48

Figure 9. Sample output waveforms of A) a normal eye’s response to the air puff, and B) a keratoconic eye with a peripheral cone’s response to the air puff48

Chapter 1. Introduction

Keratoconus

Keratoconus is a bilateral, although asymmetric, corneal ectasia, in which the corneal stroma focally thins and steepens, forming a conical shape. The location and morphology of the cone dictates its clinical classification either as a nipple cone or as an oval cone. Nipple cones are smaller in diameter than an oval cone, and they tend to be located in the central cornea, within several millimeters of the visual axis. Oval cones are located in the inferotemporal portion of the cornea, further from the visual axis than a nipple cone when evaluated using axial topography maps (Perry et al., 1980). The disease process commonly begins in early adulthood (Rabinowitz, 1998) and progresses until middle age, at which time progression slows due to the stiffening of the cornea during the normal aging process (Elsheikh et al., 2007).

The prevalence of keratoconus in the general population of the United States has been frequently cited as 1 in 2,000, based on a study analyzing keratoconus diagnoses from 1935-1982 (Kennedy et al., 1986). This study may underestimate true prevalence, however, because it was conducted before the development of corneal imaging technologies, including corneal topography and Scheimpflug tomographic imaging, both of which show corneal steepening and thinning in the absence of slit-lamp and refractive findings, which are not present in all eyes with keratoconus. A study by Naderan et al.

found corneal protrusion, scissoring reflex, corneal thinning, Fleischer's ring, and prominent nerve fibers were the most prevalent clinical findings in keratoconic corneas, and had an incidence of only 71.7%, 64.2%, 56.6%, 55.5% and 54.7%, respectively, among the keratoconic eyes. Positive biomicroscopy findings were also associated with high mean curvature, with high anterior and posterior elevation, and with thin corneal thickness, as measured with corneal topography, suggesting that slit-lamp findings are associated with severe disease and that topographic/tomographic changes may occur before manifestations on biomicroscopy (Naderan et al., 2018). A more recent study, conducted in 2017 in the Netherlands, found the incidence of keratoconus to be 5-fold to 10-fold higher than what was found in the study previously mentioned (Godefrooij et al., 2017). Sophisticated diagnostic devices are widely available in the Netherlands, and access to care is high among the population (Godefrooij et al., 2017). Incidence of keratoconus may be under-reported in countries with less accessibility to diagnostic technologies and healthcare.

Keratoconus is a multifactorial disease with various genetic and environmental risk factors. Mechanical trauma to the eye, such as that from eye rubbing or hard contact lenses, is a significant environmental factor in keratoconus development (Gasset et al., 1978). The exact mechanism by which trauma induces keratoconus is not fully understood, but some have suggested that trauma to the corneal epithelium leads to apoptosis of the underlying keratocytes (Wilson et al., 1996). Specifically, repeated corneal trauma induces apoptosis of corneal stromal fibroblasts (Wilson et al., 1996). It also increases the release of IL-1 within the cornea. IL-1 activates collagenases within the

cornea, causing breakdown of collagen within the stroma (Bureau et al., 1993). To compound the problem, the keratocytes of ectatic corneas have four times more IL-1 receptors compared to keratocytes of normal corneas (Bureau et al., 1993), which makes the former especially vulnerable to abnormal collagen production and maintenance (Bron & Rabinowitz, 1996).

Consistent with a pathophysiology based on apoptosis, some describe keratoconus as a non-inflammatory disease (Krachmer et al., 1984); however, several studies demonstrate that inflammatory processes may also contribute to development of the condition. Ultraviolet light and mechanical trauma due to eye rubbing or hard contact lenses lead to the accumulation of reactive oxygen species (ROS) within the corneal stroma (Wojcik et al., 2013). To make matters worse, keratoconic corneas have low concentrations of aldehyde dehydrogenase and superoxide dismutase enzymes, which protect the cornea from reactive aldehydes and ROS (Cristina Kenney & Brown, 2003; Wojcik et al., 2013). Excess ROS combined with a cornea ill-equipped with sufficient enzymes for eliminating ROS may play a significant role in the pathogenesis of keratoconus.

There are risk factors for keratoconus other than corneal trauma. Keratoconus affects both sexes, although it is unclear whether it is more prevalent in males or females. Keratoconus is most prevalent in patients of South Asian and Middle Eastern descent, but it can affect people of all ancestries (Santodomingo-Rubido et al., 2022). Connective tissue disorders including Ehlers-Danlos Syndrome, osteogenesis imperfecta, joint hypermobility, and mitral valve prolapse have been associated with keratoconus

(Romero-Jimenez et al., 2010). Patients with a family history of keratoconus have a higher risk of developing the disease themselves than patients without a family history of keratoconus. A study by Wang et al. found the prevalence of keratoconus in first degree relatives to be 3.34%, which is 15–67 times higher than the general population (Wang et al., 2000). The inheritance pattern of keratoconus remains unclear (Gonzalez & McDonnell, 1992; Wang et al., 2000).

Management of Keratoconus

As keratoconus progresses, intra-eye asymmetrical steepening and distortion of the cornea may occur. In early-to-moderate stages of the disease, glasses or rigid contact lenses may be used to correct vision. However, in advanced keratoconus, these options may fail to correct vision due to the presence of irregular astigmatism, aberrations of the cornea, and/or corneal scarring (Gordon-Shaag et al., 2015). Penetrating keratoplasty (PK) or deep anterior lamellar keratoplasty (DALK) may be performed to improve vision at this stage of the disease (Henein & Nanavaty, 2017). Although surgical interventions for keratoconus may preserve vision, they are associated with a wide range of post-operative complications (Asimakis & Kirkness, 1996) that may impart substantial economic burden (Chan et al., 2020) and that may lead to a diminished quality of life (Al Zabadi et al., 2023). DALK offers a non-penetrating method of corneal transplantation and has a reduced rate of rejection and refractive astigmatism in comparison to PK (Henein & Nanavaty, 2017). However, DALK, like PK, may still lead to adverse events including ocular hypertension and endothelial cell density loss over time (Borderie et al., 2023). Moreover, some studies suggest that DALK is associated with poorer visual

outcomes than PK (Henein & Nanavaty, 2017), and patients who undergo DALK still requires lifelong monitoring and anti-rejection therapy. Thus, there is a need to avoid corneal transplantation when possible.

This need at least partially is filled through corneal crosslinking. In this procedure, riboflavin and UV-A light promote covalent bond formation between collagen fibers within the corneal stroma (Randleman et al., 2015). The result is stiffening and stabilization of the cornea. Corneal crosslinking slows the progression of keratoconus and lowers the risk of needing corneal transplantation when administered early enough in the disease process (Hersh et al., 2017). Other benefits include decreased maximum keratometry values, increased corrected visual acuity, and increased uncorrected visual acuity. Adverse effects may include corneal haze, endothelial folds, and irregular epithelium (Hersh et al., 2017).

It is important to administer corneal crosslinking relatively early in the disease process. The procedure is most effective in corneas with sufficient corneal stroma thickness prior to surgery (Kreps et al., 2021). The Dresden protocol for corneal crosslinking suggests a minimum corneal thickness of 400 microns to avoid endothelial injury during radiation (Ashwin & McDonnell, 2010). Newer approaches have been developed that allow for treatment of corneas thinner than 400 microns by swelling the cornea to over 400 microns with hypoosmolar riboflavin solutions and reducing the applied UV-energy (Borgardts et al., 2023). Hafezi and colleagues have developed an additional approach known as the “Sub400 Protocol,” which adapts the magnitude of UV irradiance to the stromal thickness of the patient. This approach has been shown to halt

progression of keratoconus in eyes with corneal thickness as low as 214 microns with no signs of endothelial decompensation (Hafezi et al., 2021).

Diagnosis and Assessment of Keratoconus

Clinical signs of keratoconus seen upon slit lamp examination can be helpful in diagnosing keratoconus. Signs that may arise earliest in the disease include Fleischer's ring, which is an iron deposition that forms in a ring formation around the cone, and Vogt's striae, which are vertical lines in the posterior stroma and in Descemet's membrane. Clinical signs that typically occur later in the disease can include Munson's sign, which occurs when the lower lid takes on a V-shape in downward gaze, and Rizutti's sign, which occurs when a focused beam of light forms on the nasal limbus upon lateral illumination of the cornea (Rabinowitz, 1998).

As mentioned earlier, slit lamp biomicroscopy is insensitive to early corneal pathology. In a study done by Kreps et al, only 13% of keratoconus cases were diagnosed using biomicroscopy before the age of 18, even though disease progression begins in early-to-late teens (Kreps et al., 2021). Thus, other diagnostic tests are needed to identify the disease during its earliest stages to prevent vision loss. One such test is Placido-disc corneal topography, which is patient-friendly and easy to administer. Concentric black and white rings are reflected off the central 8-10 mm of the cornea. Analysis of the separation of the rings generates a curvature map of the anterior corneal surface (Zhang et al., 2021). A keratoconic cornea with manifest disease will show focal steepening, with accompanying focal thinning, in the location of the cone. Nicula reports that corneal

topography has high specificity (92%) and sensitivity (87%) for keratoconus (Nicula CA, 2022). Moreover, another study found that several diagnostic indices that describe the front surface of the cornea were successful in identifying the disease in approximately 90% of a cohort of eyes that previously had been diagnosed with keratoconus using other methods (Faria-Correia, 2012).

Corneal topography is not without challenges and drawbacks. Poor quality of the tear film and lid artifact may interfere with the reconstruction of the reflected image of the concentric rings in Placido-disc imaging. Corneal warpage caused by gas permeable contacts lenses can obfuscate the normal contour of the anterior cornea, potentially limiting the ability of clinicians to detect true pathology (Zhang et al., 2021). Most importantly, corneal changes due to keratoconus may begin at the posterior corneal surface (Gomes et al., 2015). That is, posterior corneal surface steepening may occur in the presence of an apparently healthy anterior corneal surface (Martin, 2018). In a study done by Faria Correia et al., anterior-surface indices did not detect 10% of keratoconic eyes in a cohort of patients with previously diagnosed disease (Faria-Correia, 2012). The anterior surface appears unaffected due to compensatory adaptation of the corneal epithelium in response to early anterior stromal surface changes. That adaptation includes epithelial thinning in the apex region of the cone with an annulus of epithelial thickening surrounding the cone, which can mask the steepening curvature (Franco et al., 2020). Lack of vision changes at this stage may also delay diagnosis, as changes to the posterior surface of the cornea have less impact on vision in comparison to changes to the anterior

surface due to the stronger refracting power of the anterior surface than of the posterior surface.

Therefore, mapping of the posterior surface may be necessary in detecting early, subclinical keratoconus before uncorrectable vision impairment arises (Gomes et al., 2015). Corneal tomography is a corneal imaging modality that assesses the anterior and posterior surfaces of the cornea. It has the potential to address some of the limitations of corneal topography. Scheimpflug imaging is a common form of corneal tomography. A Scheimpflug camera takes cross sectional images of the cornea as it rotates 180 degrees around the cornea. The captured images are processed and analyzed to generate elevation maps both of the anterior and of posterior surfaces of the cornea (Moshirfar et al., 2019). Faria-Correia and colleagues found that tomographic indices had higher sensitivity in diagnosing keratoconus compared to topographic indices, due to front surface curvature indices being normal in some eyes with mild keratoconus (Faria-Correia, 2012). Similarly, a study performed by Du et al. showed posterior elevation value as the best distinguishing index between patients with subclinical keratoconus and controls (Du et al., 2015).

Despite its advantages over corneal topography, corneal tomography has important limitations to consider. One disadvantage of Scheimpflug imaging is its long image acquisition time, approximately 2 seconds, which is comparably longer than the milliseconds measurement time of Placido-disc topography. Eye movements that occur during the 2 seconds of image acquisition have the potential to cause artifacts in the resultant corneal image. Another limitation is that Scheimpflug imaging generates

relatively few data points in the periphery of the scan; a topographical image provides equal data in the periphery as it does in the center. Finally, early diagnosis of keratoconus either with tomography or with topography is limited due to lack of uniform diagnostic criteria (Zhang et al., 2021). Additional data on the health of the cornea may enhance the ability of clinicians to detect keratoconus.

Corneal Biomechanics

Measurement of the biomechanical parameters of the cornea may supplement traditional means of keratoconus detection and assessment. The biomechanical properties of the cornea define how corneal tissue responds to stresses applied to it. Currently, two tonometers can measure *in vivo* biomechanical parameters of the human eye, the Ocular Response Analyzer (ORA) and the Corvis ST. Both devices apply a puff of air to the cornea and measure the corneal deformation response to this applied load. There are several variables that impact the cornea's response to the air puff and thus must be considered when interpreting biomechanical parameters. Intraocular pressure (IOP) is the variable that has the largest impact on biomechanics parameters because it applies a constant stress to the cornea. As IOP increases, the eye manifests a stiffer response to the applied load (Marcos, 2010). Inherent corneal stiffness is a second variable that impacts biomechanics. Corneas undergoing corneal crosslinking show less deformation to an air puff after the procedure than before it (Marcos, 2010). Central corneal thickness also impacts corneal biomechanics; a thin cornea is expected to deform more in response to an air puff than a thick cornea (Yuhua & Roberts, 2023). This has been demonstrated in cases of after small incision lenticule extraction (SMILE) refractive surgery. Corneas

have a larger deformation amplitude to an air puff after SMILE, compared to before the surgery, when the cornea was at its original thickness (Fernandez et al., 2016). Therefore, IOP, corneal stiffness, and central corneal thickness must be considered when interpreting ocular biomechanical measurements.

Ocular Response Analyzer

Clinical assessment of the biomechanical properties of the cornea requires the application of a load, such as an air puff, to the corneal surface. The aforementioned ORA (Reichert, Depew, NY) is a commercial instrument that uses an air-puff to deform the cornea. The cornea moves inward with the initiation of the air puff. It applanates and then takes on a slight concavity as the pressure of the air puff increases. When the air puff stops, the pressure exerted on the cornea decreases, and the cornea moves back outward, past a second applanated state before returning to its original convex shape.

During the deformation response, an infrared beam of light is reflected off the corneal surface and onto a photodetector. Detection of the number of photons reflected off the corneal surface and onto the photodetector allows for the generation of a waveform that represents the cornea's response to the air puff (Luce, 2016). The x-axis of the waveform indicates time, and the y-axis indicates number of photons counted by the photodetector (red trace) and the pressure generated by the air piston within the device nozzle (green trace). The most prominent features of the photon waveform are its two peaks, which represent the two appplanation events – one while the cornea is moving inward and the other while the cornea is moving outward. The most photons reflect off

the corneal surface and into the photodetector when the cornea is applanated, generating the two peaks. The valley between the peaks represents the period during which the cornea is moving from its first applanated state, to a concave formation, and back towards its second applanated state. The bottom-most point of the signal between the peaks represents the cornea's "most" concave state.

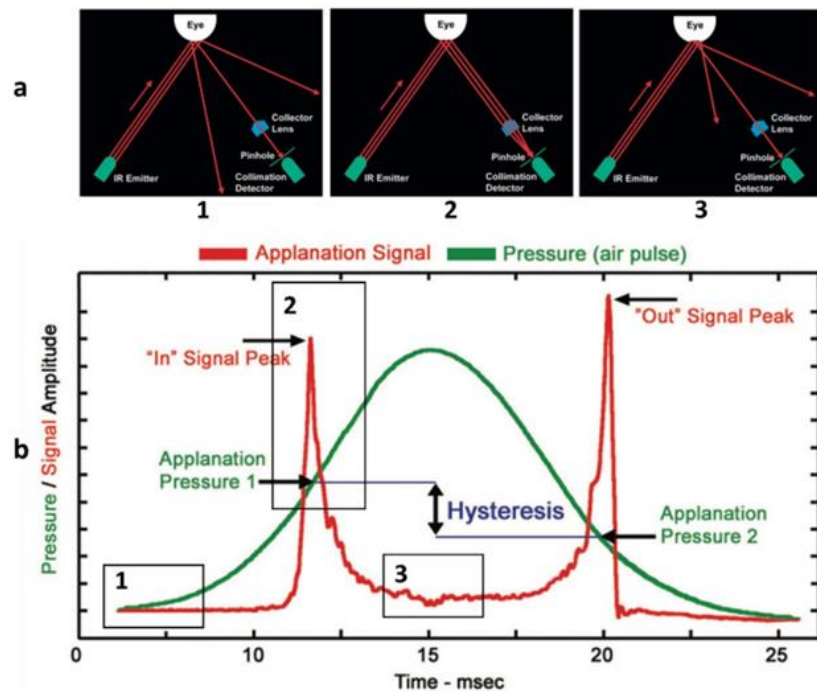


Figure 1. Generation of the ORA Waveform. **a)** Visual representation of the electro-optical detection system of the ORA 1) before applanation 2) at first inward applanation 3) at concavity **b)** A typical infrared (IR) signal (red) and the pressure signal (green) versus time 1) before applanation 2) at first inward applanation 3) at concavity. The absolute value of the IR signal is shown since both convex (positive) and concave (negative) corneal curvatures disperse the incident IR light similarly. Figure modified from Luce and Taylor, 2016.

Biomechanical Parameters

Analysis of this waveform and of the pressures at which the applanation events occur generates two metrics of intraocular pressure and characterizes several biomechanical response parameters of the eye. Pressure is measured twice, at the first and second points of applanation (P1 and P2, respectively). The average of these two pressures produces a Goldmann-correlated IOP (IOPg) value. A corneal-compensated IOP (IOPcc) value is also empirically derived from the two applanation pressures. IOPcc attempts to compensate for corneal influence on IOP (Luce, 2016).

In addition to IOPcc and IOPg, the two pressure measurements can also generate biomechanical parameters. The first is corneal hysteresis (CH), which is defined as the difference between P1 and P2. P1 is larger than P2 for all reliable measurements, so the difference between P1 and P2 yields a positive value for CH, indicating that the eye is dampening energy. CH is a whole-eye measurement, including responses of the cornea and of sclera (Yuhas & Roberts, 2023). Thus, the entire corneoscleral shell contributes to the measured magnitude of CH. The ORA also supplies a value known as corneal resistance factor (CRF), which is derived from P1 and P2 and characterizes the viscoelastic response of the cornea weighted by elasticity (Luce, 2016). Both CH and CRF are lower in patients with keratoconus than in healthy control patients (Fontes et al., 2010; Ortiz et al., 2007). However, CH and CRF poorly differentiate keratoconic corneas from normal corneas due to significant overlap in the distribution of these values between the two (Fontes et al., 2010). Other diagnostics metrics are needed.

Keratoconus Match Index

Although corneal hysteresis and corneal resistance factor have limited diagnostic potential in keratoconus, there are 37 other parameters that describe the ORA waveform and that may contribute to keratoconus detection. The study of these waveforms and of their potential to aid in keratoconus detection is in its infancy, but early results are promising. On visual inspection, the peaks of the waveforms recorded from eyes with keratoconus tend to be blunted in comparison to those recorded from healthy eyes (Figure 2). Thus, analysis of the shape of the ORA waveform parameters in healthy eyes and in keratoconic eyes may generate metrics to differentiate the two that are more sensitive than CH and CRF.

The Keratoconus Match Index (KMI) is one attempt to harness the potential of the 37 ORA waveform parameters in order to distinguish normal eyes from keratoconic eyes. KMI was developed using univariate t-tests to compare differences in the mean values of each waveform parameter between a population of normal eyes and a population of keratoconic eyes. The seven waveform parameters with the largest differences between the cohorts were identified as CRF, p2area, dslope1, h2, p2area1, h21, and waveform score, which is a measurement-quality indicator (Table 1). The KMI combines these seven parameters into a single metric, which represents risk of keratoconus. Labiris et al, 2013 studied the KMI's diagnostic ability in patients with known keratoconus. The KMI presented an overall predictive accuracy of 97.7%, with a sensitivity of 91.18% and specificity of 94.34% (Labiris et al., 2013). Labiris and colleagues further explored the potential of the KMI in a second study, which evaluated the diagnostic accuracy of KMI

in a cohort of eyes with subclinical or suspected keratoconus. The KMI showed a predictive accuracy of 94% in these eyes (Labiris et al., 2014). These results suggest that KMI is a useful tool for the evaluation of eyes with keratoconus or of eyes with suspected keratoconus.

The KMI was developed using an early-generation model of the ORA, the G1 ORA. A new-generation ORA model, the third-generation ORA (G3 ORA), has since been developed. The air puff of the G3 ORA differs from that of the old-generation models due to updates in the mechanical and optical systems of the new device, as well as improvements to its air jet. The working distance has also decreased from 11.3 mm to 8.3 mm (Luce, 2016). These differences altered the morphology of the waveform generated by the G3 ORA in comparison to the G1 ORA. As a result, KMI was not included on the new generation device, and an updated KMI was never released for the G3 ORA. Moreover, it has not been evaluated whether the original KMI is effective in identifying keratoconic eyes when using the G3 ORA, leaving a gap in our ability to detect early keratoconus using a purely biomechanical approach. **Therefore, the initial aims of this study were 1) to quantify differences in intraocular-pressure and biomechanical parameters, both between two versions of the device and between subjects with keratoconus and controls; and 2) to evaluate the performance of the original KMI in identifying keratoconic eyes when applied to G3 ORA measurement data.**

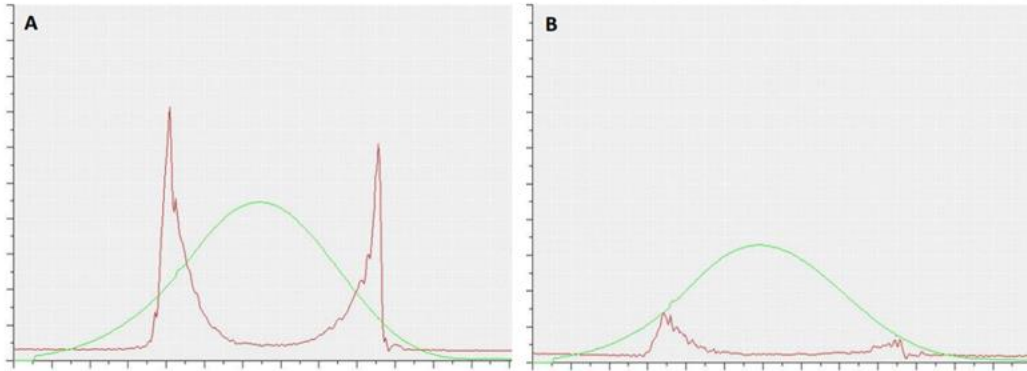


Figure 2. Sample G1 ORA waveforms from (A) a control subject and (B) a case subject. The y-axis is number of photons aligned with the detector of the device, and the x-axis is time (ms). The green trace is air pressure created by the piston of the device. The red trace is the number of photons reaching the detector. Figure from Fortman et al. 2023.

ORA Parameter	Description
<u>IOPg</u>	Goldmann correlated IOP
<u>IOPcc</u>	Corneal compensated IOP
CH	Corneal hysteresis
CRF	Corneal resistance factor
p1area	Area of applanation peak, 25%base – peak1
p2area	Area of applanation peak, 25%base – peak2
w1	Width of applanation peak, 25% base – peak1
w2	Width of applanation peak, 25% base – peak2
h1	Height of applanation peak, 25% base – peak1
h2	Height of applanation peak, 25% base – peak2

Table 1. Describes several of the 37 waveform parameters derived from an ORA waveform that are more commonly reported in the literature.

Cone Location

The location of the apex of the corneal cone differs among patients with keratoconus, usually ranging from the central cornea to its inferior quadrants, as has been shown by axial, tangential, and elevation topographical maps (Eliasy et al., 2020; Steinwender et al., 2022). The exact location of the conical apex has clinical implications, influencing the design of gas-permeable contact lenses (Sorbara et al., 2010), the placement of intracorneal ring segments (Colin et al., 2000), and the location of corneal cross-linking therapy (Greenstein et al., 2012). Moreover, visual-acuity recovery after cross-linking therapy may be greater in patients with central cones than in those with peripheral cones (Mimouni et al., 2021; Shetty et al., 2015). It is unclear, however, if the location of the cone impacts the biomechanical parameters of the cornea. That is, given similar stages of disease severity, will the centrally measured biomechanical parameters of a patient with a central cone differ from those of a patient with a peripheral cone?

Past studies have shown that collagen fibril orientation is disrupted around the apex of the cone, suggesting that lamellar weakening in keratoconus is focal and not global in nature (Meek et al., 2005). Finite element modeling has identified loss of tissue stiffness, which is localized to a concentric area around the cone, as a contributor to keratoconus progression (Falgayrettes et al., 2023), and several groups have used Brillouin microscopy, a form of non-destructive optical elastography (Prevedel et al.,

2019), to demonstrate focal, not global, weakness in keratoconus that is associated with local corneal thinning and steepening (Scarcelli et al., 2015; Scarcelli et al., 2014; Shao et al., 2019). This evidence for isolated areas of lamellar weakening supports the theory put forth by Roberts & Dupps (Roberts & Dupps, 2014) that focal biomechanical weakening is the primary event in the development of keratoconus. The focal nature of this condition results in asymmetry in the biomechanical properties of the cornea, so it is expected that corneas with central cones will exhibit a different biomechanical response, as measured by the ORA, than corneas with peripheral cones.

The theory that central cones exhibit different biomechanical responses than peripheral cones has been studied using an instrument called the Corvis ST (OCULUS, Wetzlar, Germany), which delivers an air puff to the cornea similarly to the ORA but uses real-time Sheimpflug imaging to analyze the biomechanical deformation response of the cornea to the air puff. Bruner et al. showed that all biomechanical metrics of central corneal stiffness as measured by the Corvis ST increase as the cone distance from center increases (Bruner C, 2022). However, cone location impact on biomechanics of the cornea has never been tested using the ORA. Therefore, **the third purpose of this study is to investigate whether cone location influences the ORA-measured biomechanical parameters of the cornea in keratoconus.**

Chapter 2. Methods

Ethics Statement

The study was approved by The Ohio State University (OSU) Institutional Review Board, and all subjects gave written informed consent before participating.

Subject Recruitment and Inclusion Criteria

Fifty subjects (n = 50) with previously diagnosed keratoconus (ICD-10 code root H18.6) and 144 healthy control subjects (n = 144) were prospectively recruited from the OSU optometry clinics and from the local community. Exclusion criteria for the keratoconus group included: 1) age under 18 years; 2) diseases of the cornea other than keratoconus (KCN); 3) glaucoma and other optic neuropathies; 4) ocular hypertension; 5) diabetes mellitus; 6) history of ocular surgeries other than cataract surgery; and 7) current use of orthokeratology contact lenses. These exclusion criteria also were applied to control participants, save that control could not have a diagnosis of KCN in either eye.

Data Collection

All subjects sat for a single study session. First, subjects provided their age and self-identified ancestry. Then, axial and tangential corneal topography maps were collected from both eyes using an E300 Corneal Topographer (Medmont; Nunawading, Australia). Measurements of IOP and of biomechanical parameters were made using two

Ocular Response Analyzer air-puff tonometers (ORA; Reichert; Depew, NY): the G1 ORA model and the G3 ORA model. Four consecutive measurements were taken from each eye with each ORA. The old-generation ORA G1 required each measurement to be taken separately by pressing a button on the ORA computer interface; in contrast, the ORA G3 took four measurements automatically in rapid succession. The order of data collection from the two ORA devices was randomized to control for any potential order effect.

Inter-device Differences

Outcome Measures

IOP outcome measures produced by both generations of the ORA included IOPcc and IOPg. Biomechanical outcome parameters produced by both generations of the ORA included CH, WS, p1area, p2area, w1, w2, h1, h2, and KMI (Table 1). Specifically, p1area and p2area represent the area under the curve of the first and second applanation peaks, respectively, from a plane 25% above baseline, which is defined as the nadir of the valley between the two applanation peaks (Figure 3a). W1 and w2 represent the width of the first and second applanation peaks, respectively, at a point 25% above baseline (Figure 3b). H1 and h2 represent the height of the first and second applanation peaks, respectively, measured from a plane 25% above baseline (Figure 3c). These waveform parameters were specifically chosen among the 37 available parameters because they are most easily interpreted and characterize applanation characteristics of the eye's deformation response. Software for calculating parameters on G1 ORA and G3 ORA was provided by Reichert.

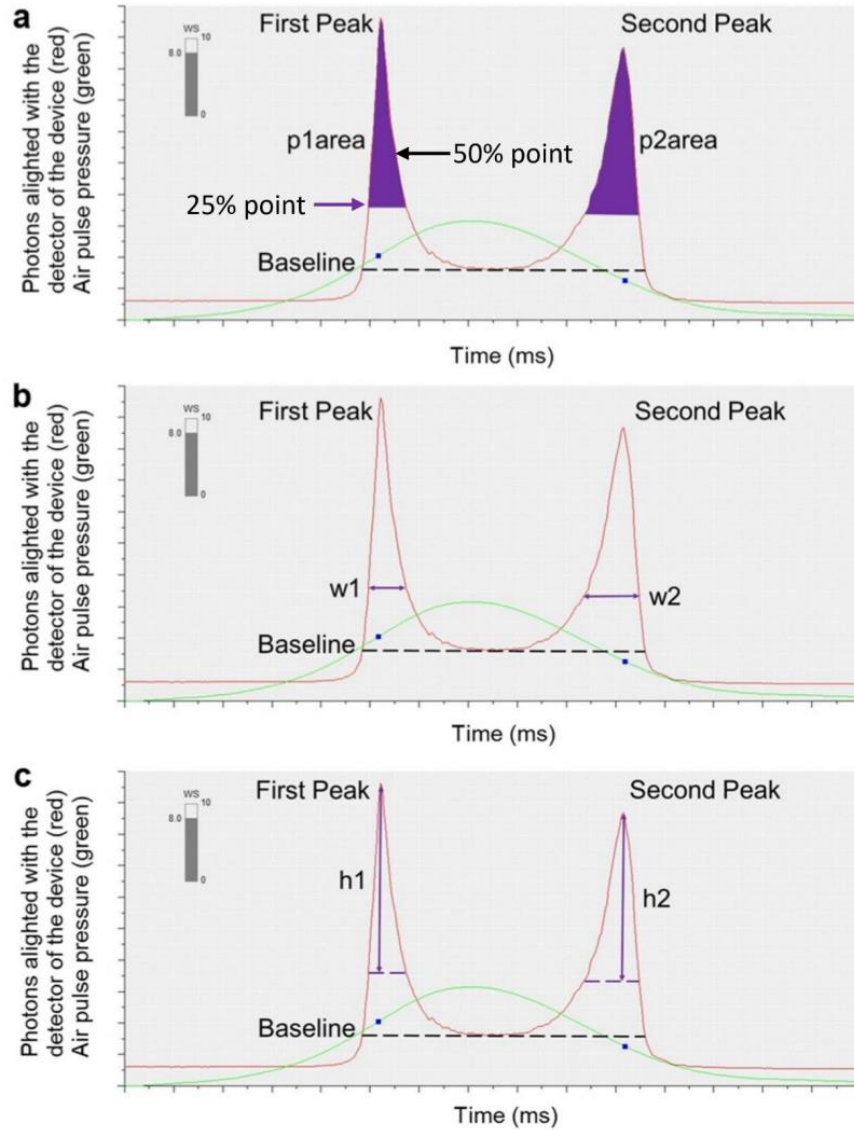


Figure 3. Example waveform parameters. (a) Area of the first peak (p1area) and area of the second peak (p2area), (b) width of the first peak (w1) and width of the second peak (w2), and (c) height of the first peak (h1) and height of the second peak (h2) parameters identified on a representative pressure-applanation waveform generated by the Ocular Response Analyzer. The green traces represent the air pressure delivered to the cornea. The red traces represent the number of photons reflected off the corneal surface and into the infrared light sensor. Peak 1 occurs during first corneal applanation, which happens during inward deformation; and Peak 2 occurs during second corneal applanation, which happens during the outward recovery after cessation of the air puff. The waveform parameters are indicated in purple. The dark blue solid boxes mark the location along the pressure curve where the peaks of the infrared waveform occur. Figure from Yuhas et al., 2024.

Statistical Analysis

For both devices, the measurement with the highest waveform score from each eye was selected for data analysis. Given the known asymmetry in disease severity and in biomechanical parameters between the eyes in keratoconus (Zadnik et al., 2002) both eyes of each case subject were included in the case cohort. In contrast, only the left eye of each control subject was included in the control cohort, as eyes without disease may be more likely to produce similar biomechanical properties. All outcome measures were compared between the two generations of ORAs using paired t-tests and between cohorts using t-tests. Significance threshold for inter-device difference comparisons was set at $\alpha = 0.002$ (Bonferroni correction) to account for multiple comparisons.

Cone Location

Data Processing

Only eyes in the keratoconus group were considered in this portion of data processing. For all eyes, cone location was defined as the center of a 2 mm circle of maximum curvature, following an objective, published search algorithm, which searches over a defined region of interest to identify a 2 mm area of maximum tangential and axial curvature in diopters (Mahmoud et al., 2008). Average magnitude of corneal curvature within this 2 mm area was defined as Cspot. Disease severity was defined as the magnitude of Cspot on the tangential curvature map. Then, eyes were grouped into four cohorts, based on cone location and on type of topography map used to identify the location of the cone. The four cohorts included: 1) axial central-cone cohort; 2) axial peripheral-cone cohort; 3) tangential central-cone cohort; and 4) tangential peripheral-

cone cohort. For axial topography, the central-cone cohort included cones with the center of Cspot located within a 1.5 mm radius from the center of the cornea (i.e., within the central 3 mm of the cornea), and for the axial peripheral-cone cohort, the center of Cspot was located outside a 1.5 mm radius from the center of the cornea (i.e., outside the central 3 mm of the cornea). For tangential topography, the center of Cspot was located within a 1.5 mm radius from the map center for the central-cone cohort, and outside a 1.5 mm radius from the center of the cornea for the tangential peripheral cone cohort. Keratometry values (flat meridian, steep meridian, and corneal cylinder) were also recorded from the axial topography map. Only topography maps without artifact on visual inspection were included in data analysis.

Similar to above, individual eyes of all participants with keratoconus were treated independently. If one eye had a central cone, and the fellow eye had a peripheral cone, then the two eyes were binned into separate cohorts. If both eyes had central cones, or if both eyes had peripheral cones, then the eyes were binned into the same appropriate cohort. Data from the ORA measurement with the highest waveform score were analyzed for each eye. In addition to the standard clinical output parameters of waveform score and CH, waveform parameters p1area, p2area, w1, w2, h1, and h2 were exported from the twin-peaked pressure-applanation waveforms generated by the device.

Statistical Analysis

Unpaired t-tests were used to compare differences in WS, CH, p1area, p2area, w1, w2, h1, and h2 between the central-cone cohort and the peripheral-cone cohort in both curvature cohorts (Statistical Analysis Software; SAS Institute, Cary, NC, USA).

Cspot magnitude was compared for tangential topography only; and the steep-meridian keratometry value, the flat-meridian keratometry value, and corneal cylinder were compared for axial topography. Normality was confirmed with the Shapiro–Wilk test. Associations between cone location, as defined both by axial topography and by tangential topography, and WS, CH, p1area, p2area, w1, w2, h1, and h2 were assessed with linear regression analyses. Very weak associations were defined as $r \leq 0.19$, weak associations were defined as r between 0.2 and 0.39, moderate associations were defined as r between 0.4 and 0.59, strong associations were defined as r between 0.6 and 0.79, and very strong associations were defined as $r \geq 0.8$. For all statistical analyses regarding cone location, the significance threshold was set at $\alpha = 0.05$.

Chapter 3. Results

Inter-device and Inter-cohort Differences with G1 ORA and G3 ORA

Demographics

Table 2 contains the demographic characteristics of the case and control cohorts. There were 78 eyes in the case cohort and 144 eyes in the control cohort. The controls had a higher mean age than the cases. The subjects in the case cohort were predominantly male, but the patients in the control cohort were predominantly female. Race and ethnicity varied among both cohorts.

	Cases (n = 78 eyes)	Controls (n = 144 eyes)
Age (years)	38 ± 13	39 ± 17
Sex (% female)	28	61
% White	58	81
% Black	32	6
% Mixed Race	6	2
% Hispanic	4	1
% Asian	0	7
% Unknown	0	2

Table 2. Demographic characteristics of case and control participants. Values are mean ±SD, unless otherwise noted.

Differences in IOP and Biomechanical Parameters Between G1 ORA and G3 ORA in Case and Control Cohorts

Table 3 contains the differences in outcome metrics between the G1 ORA and the G3 ORA in the case cohort. The G3 ORA measured significantly greater CH, WS, p1area, p2area, h1, h2, w2, and KMI compared to the G1 ORA. The G1 ORA measured significantly greater w1 than the G3 ORA. There were no statistically significant differences in IOPcc and IOPg between the two devices.

Table 4 contains the differences in outcome metrics between the G1 ORA and the G3 ORA in the control cohort. The G3 ORA measured significantly greater CH, WS, p1area, p2area, h1, h2, w2, and KMI than the G1 ORA. The G1 ORA measured statistically significant greater w1 than the G3 ORA. There were no statistically significant differences in IOPcc and IOPg between the two devices.

Bland- Altman plots comparing IOPcc, IOPg, CH, WS, p1area, p2area, w1, w2, h1, and h2 between the G1 ORA and G3 ORA in the case and control cohorts can be found in Appendix A.

	G1 ORA	G3 ORA	Diff (G1-G3)	P value
IOPcc (mmHg)	12.50 ± 2.822	12.47 ± 2.751	0.0308 ± 2.300	0.9063
IOPg (mmHg)	9.211 ± 3.606	9.787 ± 3.821	-0.5731 ± 2.078	0.0172
CH (mmHg)	8.628 ± 1.633	9.115 ± 1.586	-0.4872 ± 1.241	0.0009*
WS	5.696 ± 2.332	6.662 ± 1.964	-0.9660 ± 1.680	<0.0001*
p1area	2982 ± 1203	3630 ± 1437	-648.1 ± 725.8	<0.0001*
p2area	2038 ± 885.5	3903 ± 1574	-1865 ± 1227	<0.0001*
h1	322.8 ± 127.4	414.8 ± 154.8	-91.99 ± 97.62	<0.0001*
h2	289.3 ± 113.0	377.6 ± 136.9	-88.31 ± 84.43	<0.0001*
w1	23.46 ± 4.648	18.92 ± 2.443	4.538 ± 4.339	<0.0001*
w2	18.85 ± 6.207	25.17 ± 6.091	-6.321 ± 6.383	<0.0001*
KMI	0.3874 ± 0.4679	1.069 ± 0.6479	-0.6819 ± 0.4043	<0.0001*

Table 3. Differences in corneal-compensated IOP (IOPcc), Goldmann-correlated IOP (IOPg), corneal hysteresis (CH), waveform score (WS), area under first applanation peak (p1area), area under second applanation peak (p2area), height of first applanation peak (h1), height of second applanation peak (h2), width of first applanation peak (w1), width of second applanation peak (w2), and Keratoconus Match Index (KMI) as measured by the G1 Ocular Response Analyzer (ORA) and the G3 ORA in the case cohort. *p<0.002, t-test. Values are mean ± SD.

	G1 ORA	G3 ORA	Diff (G1-G3)	P value
IOPcc (mmHg)	14.45 ± 3.311	14.20 ± 3.015	0.2410 ± 2.429	0.2358
IOPg (mmHg)	14.15 ± 3.118	14.48 ± 3.095	-0.3347 ± 1.922	0.0384
CH (mmHg)	10.74 ± 1.873	11.24 ± 1.427	-0.4965 ± 1.130	<0.0001*
WS	7.573 ± 1.185	8.139 ± 0.995	-0.5665 ± 1.350	<0.0001*
p1area	4636 ± 1109	5115 ± 989.3	-479.3 ± 837.0	<0.0001*
p2area	3173 ± 918.8	6225 ± 1241	-3052 ± 1162	<0.0001*
h1	461.4 ± 70.11	528.5 ± 78.59	-67.04 ± 83.74	<0.0001*
h2	387.6 ± 80.05	515.3 ± 73.73	-127.7 ± 91.24	<0.0001*
w1	23.40 ± 2.669	20.31 ± 1.994	3.097 ± 2.661	<0.0001*
w2	20.47 ± 4.066	27.42 ± 3.707	-6.951 ± 4.136	<0.0001*
KMI	0.9878 ± 0.3295	1.899 ± 0.3458	-0.9116 ± 0.3230	<0.0001*

Table 4. Differences in corneal-compensated IOP (IOPcc), Goldmann-correlated IOP (IOPg), corneal hysteresis (CH), waveform score (WS), area under first applanation peak (p1area), area under second applanation peak (p2area), height of first applanation peak (h1), height of second applanation peak (h2), width of first applanation peak (w1), width of second applanation peak (w2), and Keratoconus Match Index (KMI) as measured by the G1 Ocular Response Analyzer (ORA) and the G3 ORA in the control cohort. *p<0.002, t-test. Values are mean ± SD.

Differences in IOP and Biomechanical Parameters Between the Case and Control Cohorts as Measured by G1 ORA and G3 ORA

Table 5 contains the differences in G1 ORA outcome metrics between the case and control cohorts. The control cohort had significantly greater IOPcc, IOPg, CH, WS, p1area, p2area, h1, h2, and KMI than the case cohort. There were no statistically significant differences in w1 and w2 between the two cohorts.

Table 6 contains the differences in G3 ORA outcome metrics between the case and control cohorts. The control cohort had significantly greater IOPcc, IOPg, CH, WS, p1area, p2area, h1, h2, w1, and KMI than the case cohort. The only parameter that did not significantly differ between the two cohorts was w2.

	Cases	Controls	Diff (case-control)	P value
IOPcc (mmHg)	12.50 ± 2.822	14.45 ± 3.310	-1.949 ± 3.148	<0.0001*
IOPg (mmHg)	9.214 ± 3.606	14.15 ± 3.118	-4.935 ± 3.297	<0.0001*
CH (mmHg)	8.629 ± 1.633	10.74 ± 1.873	-2.116 ± 1.793	<0.0001*
WS	5.696 ± 2.332	7.573 ± 1.185	-1.877 ± 1.678	<0.0001*
p1area	2982 ± 1203	4636 ± 1109	-1654 ± 1143	<0.0001*
p2area	2038 ± 885.5	3173 ± 918.8	-1135 ± 907.3	<0.0001*
h1	322.8 ± 127.4	461.4 ± 70.11	-138.6 ± 94.19	<0.0001*
h2	289.3 ± 113.0	387.6 ± 80.05	-98.25 ± 92.93	<0.0001*
w1	23.47 ± 4.648	23.40 ± 2.669	0.0588 ± 3.492	0.9183
w2	18.85 ± 6.207	20.47 ± 4.066	-1.626 ± 4.922	0.0394
KMI	0.3874 ± 0.4679	0.9878 ± 0.3295	-0.6004 ± 0.3836	<0.0001*

Table 5. Inter-cohort differences in corneal-compensated IOP (IOPcc), Goldmann-correlated IOP (IOPg), corneal hysteresis (CH), waveform score (WS), area under first applanation peak (p1area), area under second applanation peak (p2area), height of first applanation peak (h1), height of second applanation peak (h2), width of first applanation peak (w1), width of second applanation peak (w2), and Keratoconus Match Index (KMI), as measured by the G1 Ocular Response Analyzer. *p < 0.002, t-test. Values are mean ± SD.

	Case	Control	Diff (case-control)	P value
IOPcc (mmHg)	12.47 ± 2.751	14.20 ± 3.015	-1.739 ± 2.925	<0.0001*
IOPg (mmHg)	9.787 ± 3.821	14.48 ± 3.095	-4.697 ± 3.367	<0.0001*
CH (mmHg)	9.115 ± 1.586	11.24 ± 1.426	-2.126 ± 1.484	<0.0001*
WS	6.662 ± 1.964	8.139 ± 0.9947	-1.477 ± 1.412	<0.0001*
p1area	3630 ± 1437	5115 ± 989.3	-1485 ± 1166	<0.0001*
p2area	3903 ± 1574	6225 ± 1241	-2322 ± 1367	<0.0001*
h1	414.8 ± 154.8	528.5 ± 78.59	-113.7 ± 111.4	<0.0001*
h2	377.6 ± 136.9	515.3 ± 73.73	-137.7 ± 100.5	<0.0001*
w1	18.92 ± 2.443	20.31 ± 1.994	-1.383 ± 2.162	<0.0001*
w2	25.17 ± 6.091	27.42 ± 3.707	-2.257 ± 4.682	0.0035
KMI	1.069 ± 0.6479	1.899 ± 0.3458	-0.8301 ± 0.4740	<0.0001*

Table 6. Inter-cohort differences in corneal-compensated IOP (IOPcc), Goldmann-correlated IOP (IOPg), corneal hysteresis (CH), waveform score (WS), area under first applanation peak (p1area), area under second applanation peak (p2area), height of first applanation peak (h1), height of second applanation peak (h2), width of first applanation peak (w1), width of second applanation peak (w2), and Keratoconus Match Index (KMI), as measured by the G3 Ocular Response Analyzer. *p < 0.002, t-test. Values are mean ± SD.

Ability of KMI to Differentiate Between Cases and Controls with G1 and G3 ORA

Figure 4 contains Receiver Operating Characteristic Curves demonstrating the ability of KMI to differentiate cases from controls when measuring eyes with the G1 ORA (Fig. 4A) and G3 ORA (Fig. 4B). The area under the curve is marginally greater when using KMI and the G3 ORA than when using KMI and the G1 ORA.

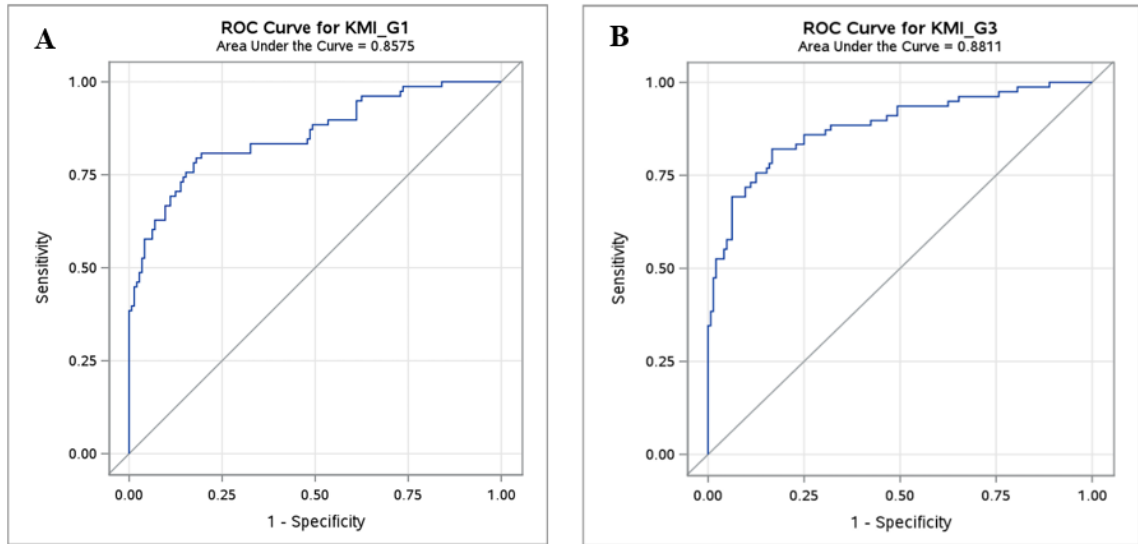


Figure 4. Receiver-operator characteristic (ROC) curves for (A) keratoconus match index (KMI) with the G1 Ocular Response Analyzer (ORA), (B) KMI with the G3 ORA.

Cone Location

Demographics

After comparing the performance of the devices, the 78 eyes in the case cohort were reanalyzed to determine the location of the cone. Figure 5a shows the location of the cones, according to the axial topography maps. For axial topography, 37 eyes had central cones, and 41 eyes had peripheral cones. There was no statistically significant difference in age ($p = 0.85$) between the central-cone cohort (38 ± 14 years) and the peripheral-cone cohort (39 ± 12 years). Figure 5b shows the location of the cones, according to the tangential topography maps. For tangential topography, 53 eyes had central cones, and 25 eyes had peripheral cones. There was no statistically significant difference in age ($p =$

0.10) between the central-cone cohort (37 ± 13 years) and the peripheral-cone cohort (42 ± 14 years).

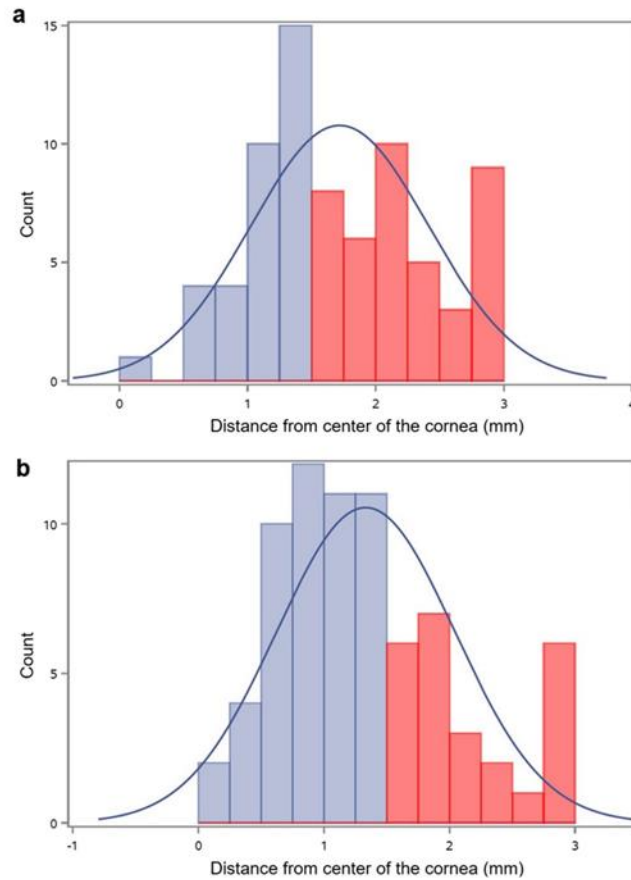


Figure 5. Cone location by cohort. Location of the cone for 78 eyes with keratoconus (a) for axial-topography and (b) for tangential-topography. Central cones (light blue) were defined as being within a 1.5 mm radius from the center of the cornea, and peripheral cones (light red) were defined as being outside of a 1.5 mm radius from the center of the cornea. The dark blue line represents the normal distribution curve. Figure from Yuhás et al. 2024.

Axial Curvature Algorithm

Keratometry Values

The steep-meridian simulated keratometry value, the flat-meridian keratometry value, and corneal cylinder were all significantly greater in the central-cone cohort than in the peripheral-cone cohort (Table 7).

Parameters	Central-cone cohort (n = 36)	Peripheral-cone cohort (n = 41)	P value
Steep-meridian keratometry value (D)	54.44 ± 10.83	47.42 ± 3.51	0.0006*
Flat-meridian keratometry value (D)	49.90 ± 9.06	44.52 ± 3.18	0.0015*
Corneal cylinder (D)	4.54 ± 3.24	2.90 ± 2.44	0.01*
Maximum tangential curvature (D)	50.93 ± 12.48	53.36 ± 6.22	0.26

Values are mean ± standard deviation. Significance threshold $\alpha = 0.05$

* $P < 0.05$, t-test

Table 7. Differences in keratometry from axial topography and maximum tangential curvature, as defined by Cspot magnitude, between central cones and peripheral cones. Table from Yuhas et al. 2024.

Differences in Biomechanical Parameters Between Central Cones and Peripheral Cones

Table 8 contains the differences in WS, CH, and waveform parameters between the central-cone and the peripheral-cone cohort for axial topography. WS, p1area, p2area, h1, and h2 were all significantly lower in the central-cone cohort than in the peripheral-cone cohort. There were no statistically significant differences between the cohorts for CH, w1, and w2.

Parameters	Central-cone cohort (n = 37)	Peripheral-cone cohort (n = 41)	P value
Waveform score	5.99 ± 1.96	7.26 ± 1.78	0.004*
Corneal hysteresis (mmHg)	8.90 ± 1.57	9.31 ± 1.60	0.26
P1area	3080 ± 1485	4127 ± 1209	0.001*
P2area	3310 ± 1490	4439 ± 1467	0.001*
W1	18.78 ± 2.46	19.05 ± 2.45	0.64
W2	25.22 ± 6.53	25.12 ± 5.75	0.95
H1	361 ± 167	463 ± 127	0.003*
H2	324 ± 124	426 ± 131	0.0007*

Values are mean ± standard deviation. Significance threshold $\alpha = 0.05$

P1area = area of the first peak; *P2area* = area of the second peak; *W1* = width of the first peak; *W2* = width of the second peak; *H1* = height of the first peak; *H2* = height of the second peak

* $P < 0.05$, t-test

Table 8. Differences in biomechanical parameters between central cones and peripheral cones for axial topography. Table from Yuhas et al. 2024.

Associations between Cone Location and Biomechanical Parameters

For axial topography, there were moderate-strength and statistically significant associations between cone location and WS ($r = 0.41$, $p = 0.0003$; Fig. 6a), between cone location and *p2area* ($r = 0.40$, $p = 0.0003$; Fig. 6b), and between cone location and *h2* ($r = 0.48$, $p = 0.001$; Fig. 6c). There were weak but statistically significant associations between cone location and *p1area* ($r = 0.34$, $p = 0.003$; Fig. 6d) and between cone location and *h1* ($r = 0.34$, $p = 0.003$; Fig. 6e). There were very weak and non-significant associations between cone location and *w1* ($r = -0.07$, $p = 0.53$; Fig. 6f), between cone location and *w2* ($r = -0.05$, $p = 0.67$; Fig. 6g), and between cone location and CH ($r = 0.13$, $p = 0.27$; Fig. 6h).

Tangential Curvature Algorithm

Keratoconus Severity

There was no statistically significant difference ($p = 0.26$) in maximum tangential curvature (Table 7), as defined by Cspot magnitude, between the central-cone cohort and the peripheral-cone cohort.

Differences in Biomechanical Parameters Between Central Cones and Peripheral Cones

Table 9 contains the differences in WS, CH, and waveform parameters between central-cone and the peripheral-cone cohorts for tangential topography. WS, p1area, p2area, h1, and h2 were all significantly lower in the central-cone cohort than in the peripheral-cone cohort. There were no significant differences between the cohorts for CH, w1, and w2.

Associations between Cone Location and Biomechanical Parameters

For tangential topography, there were weak but statistically significant associations between cone location and p2area ($r = 0.27$, $p = 0.02$, Fig. 7a), between cone location and h1 ($r = 0.23$, $p = 0.05$; Fig. 7b), and between cone location and h2 ($r = 0.25$, $p = 0.03$; Fig. 7c). There were weak and non-significant associations between cone location and WS ($r = 0.20$, $p = 0.09$; Fig. 7d) and between cone location and p1area ($r = 0.23$, $p = 0.05$; Fig. 7e). There were very weak and non-significant associations between cone location and w1 ($r = -0.05$, $p = 0.69$; Fig. 7f), between cone location and w2 ($r = 0.06$, $p = 0.62$; Fig. 7g), and between cone location and CH ($r = -0.07$, $p = 0.58$; Fig. 7h).

Parameters	Central-cone cohort (n = 53)	Peripheral-cone cohort (n = 25)	P value
Waveform score	6.34 ± 1.95	7.34 ± 1.84	0.04*
Corneal hysteresis (mmHg)	9.02 ± 1.51	9.33 ± 1.76	0.42
P1area	3356 ± 1357	4211 ± 1456	0.01*
P2area	3628 ± 1569	4488 ± 1446	0.02*
W1	18.94 ± 2.46	18.88 ± 2.45	0.92
W2	25.40 ± 6.65	24.68 ± 4.79	0.63
H1	389 ± 154	470 ± 145	0.03*
H2	348 ± 121	440 ± 150	0.005*

Values are mean ± standard deviation. Significance threshold $\alpha = 0.05$.

P1area = area of the first peak; *P2area* = area of the second peak; *W1* = width of the first peak; *W2* = width of the second peak; *H1* = height of the first peak; *H2* = height of the second peak

Table 9. Differences in biomechanical parameters between central cones and peripheral cones for tangential topography. Table from Yuhas et al. 2024.

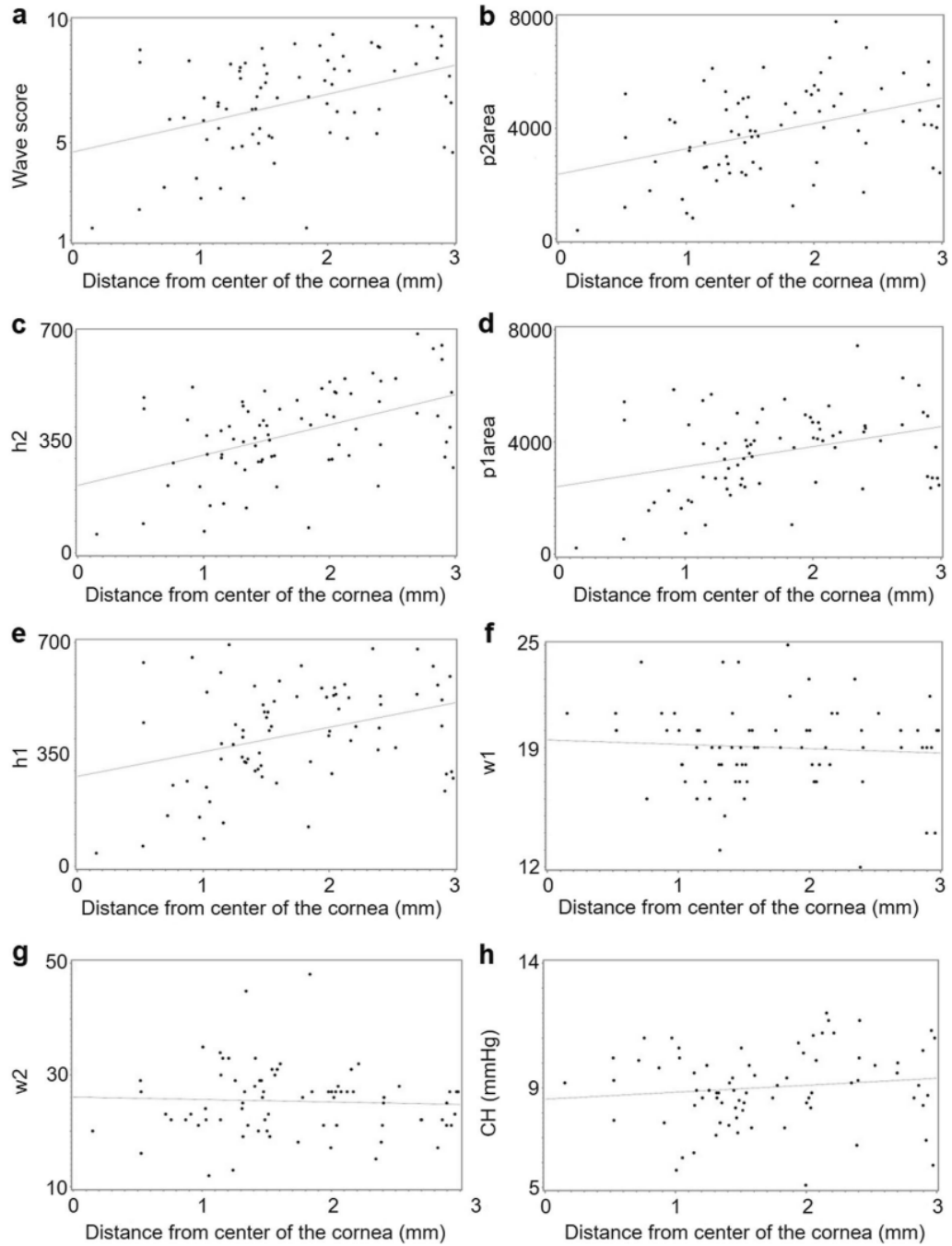


Figure 6. Associations between cone location according to axial topography and biomechanical parameters. Scatter plots showing the relationships between cone location and (a) wave score, (b) area of the second peak (p2area), (c) height of the second peak (h2), (d) area of the first peak (p1area), (e) height of the first peak (h1), (f) width of the first peak (w1), (g) width of the second peak (w2), and (h) corneal hysteresis (CH). Linear regression lines are solid gray. N=78 eyes with keratoconus. Figure from Yuhás et al. 2024.

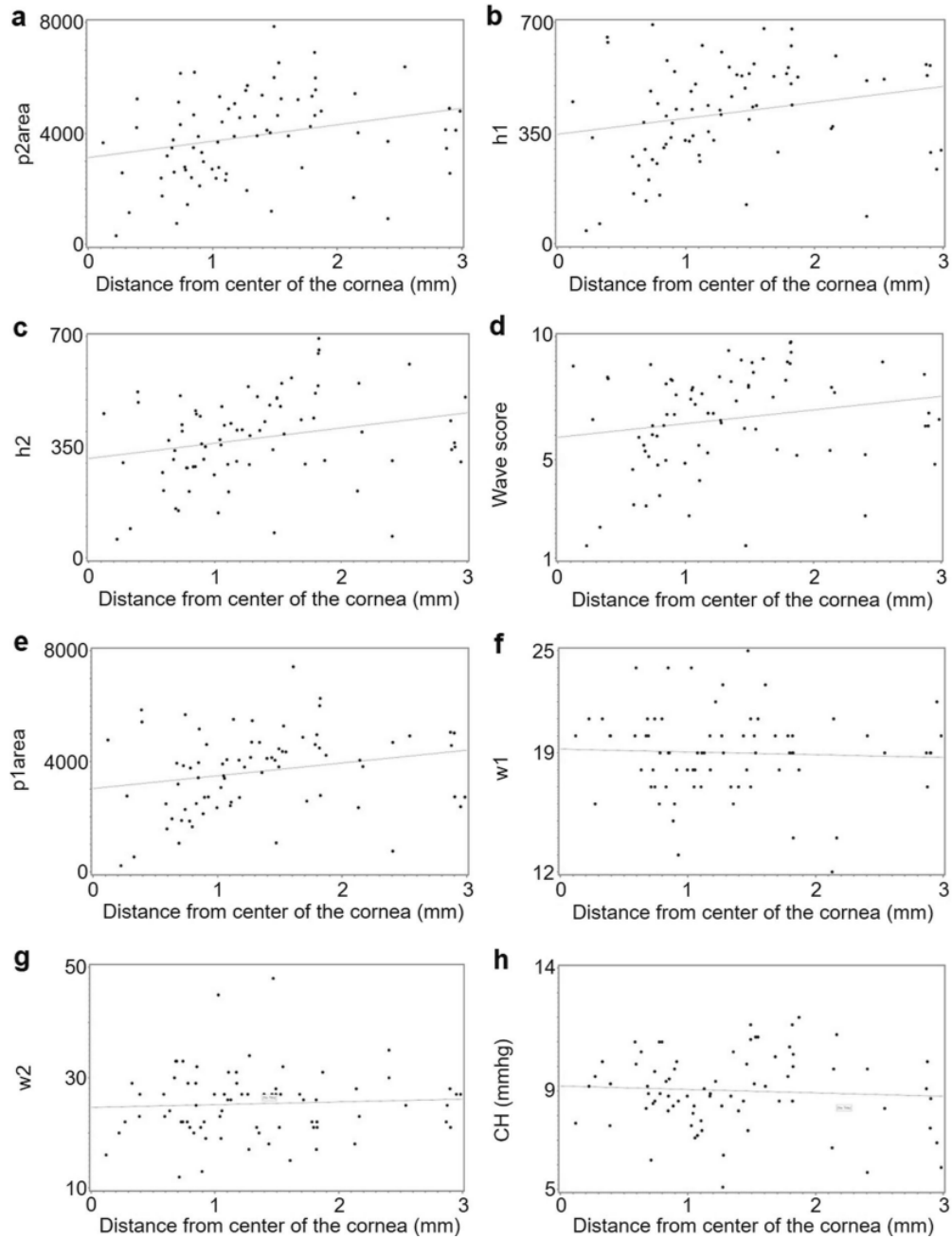


Figure 7. Associations between cone location according to tangential topography and biomechanical parameters. Scatter plots showing the relationships between cone location and (a) area of the second peak (p2area), (b) height of the first peak (h1), (c) height of the second peak (h2), (d) wave score, (e) area of the first peak (p1area), (f) width of the first peak (w1), (g) width of the second peak (w2), and (h) corneal hysteresis (CH). Linear regression lines are solid gray. N=78 eyes with keratoconus. Figure from Yuhás et al. 2024.

Chapter 4. Discussion

Differences in IOP and Biomechanical Parameters between G1 ORA and G3 ORA in Case and Control Cohorts

This study demonstrated differences in intraocular-pressure and biomechanical waveform parameters between the G1 and G3 Ocular Response Analyzer (ORA), both in case subjects with keratoconus and in healthy controls. The G3 ORA measured significantly greater corneal hysteresis (CH), waveform score (WS), area under first applanation peak (p1area), area under second applanation peak (p2area), height of first applanation peak (h1), height of second applanation peak (h2), width of first applanation peak (w2), and keratoconus match index (KMI) compared to the G1 ORA, in the case and control cohorts. The G1 ORA measured significantly greater width of first applanation peak (w1) than the G3 ORA in both cohorts. These results suggest that the air jet delivery and applanation detection system hardware changes incorporated in the G3 ORA did affect quantification of biomechanical waveform parameters, compared to the G1 ORA, in this dataset. Therefore, the G1 ORA and G3 ORA are not interchangeable devices, and caution should be taken when comparing biomechanical results between the two generations of the device. Unlike the waveform parameters, IOPcc and IOPg measurements did not significantly differ between G1 and G3 in either cohort; therefore, comparisons of IOPcc and IOPg between the devices can be made with confidence.

IOPcc attempts to provide an IOP value that is less influenced by corneal biomechanical properties, which may explain why it did not differ between the two devices.

The ORA measures the deformation response of the cornea to an air puff in an indirect manner. An infrared beam of light is directed at the cornea during the air puff, and a photon sensor detects photons reflected off the corneal surface. As the cornea moves in an inward direction and reaches its first applanated state, a high number of photons reflect off the flat corneal surface and into the photon sensor to create the first peak of the waveform. After first applanation, the cornea moves further inward into a concave state, scattering the photons. Then the air puff begins to reduce in magnitude, and the cornea follows by beginning to recover from the air puff, moving outward until it reaches a second applanated state. For a second time, a high number of photons reflect off the corneal surface into the photon sensor to create the second peak of the waveform. The cornea then returns to its original state. A large area of applanation allows many photons to reflect into the sensor, resulting in higher peaks on the waveform. Conversely, a small area of applanation results in comparatively fewer photons aligning with the sensor, resulting in lower peaks on the waveform.

Applanation area may be an indicator of corneal stiffness. Consider the analogy of two hollow spheres, sphere A and sphere B. Sphere A and sphere B are filled with the same amount of air and have the same dimensions, but the material of sphere A is stiffer than the material of sphere B. If one were to push on sphere B, it would make a deep but narrow indentation. The same force would cause a broad, but shallow indentation in sphere A, the stiffer sphere. In the same way, an ORA air puff delivered to a relatively stiff central cornea would elicit a boarder applanation area, and therefore a higher

waveform peak (Fig. 8a), than an ORA air puff delivered to a compliant central cornea (Fig. 8b).

H1, h2, p1area, and p2area are waveform characteristics that describe the two applanation events. The values of these parameters increase with higher number of photons detected by the sensor, and thus increase with broader applanation areas. The G3 ORA measured greater values for these parameters, indicating the applanation areas of corneas in the study were broader with the G3 ORA than with the G1 ORA. Therefore, these differences could be interpreted that the G3 ORA measures a stiffer response from an eye than the G1 ORA. However, it is highly unlikely that a particular eye became stiffer in the time between the G1 and G3 measurement. An alternative explanation for the G3 ORA measuring greater values for these certain biomechanical parameters is that it achieves better alignment with the apex of the cornea before delivering the air puff than the G1 ORA. The ORA has a fully automated alignment system that delivers the air puff to a precise location (Kaushik & Pandav, 2012); the operator of the ORA does not manually influence the alignment of the air puff. An air puff delivered more precisely to the apex of the cornea would cause a broader applanation area, and thus higher photon reflectivity off the corneal surface back toward the sensor, than would an applanation that is not precisely at the apex of the cornea.

WS is a quantitative representation of the quality of the measurement signal. Higher WS is associated with a more repeatable deformation response to the air puff (Luce, 2016). WS was higher with the G3 ORA in both the case and control cohort; thus, the G3 ORA produces more repeatable responses in comparison to the G1 ORA. This result suggests that the G3 ORA may be a more sensitive to changes in biomechanical

parameters of an eye over time due to relatively low inter-measurement variability. This hypothesis still needs to be tested.

The G3 ORA also measured higher CH than the G1 ORA both in the case and in the control cohorts. This result may be important to consider when evaluating patients for glaucoma risk, as high CH has been shown to reduce risk for glaucoma development and progression compared to low CH (Susanna et al., 2018). This difference between devices may be important to consider in the case of upgrading devices within a clinic that follows glaucoma patients or suspects over time. For example, it may falsely appear that a patient's CH has increased over time when they are measured by the G3 ORA, compared to when they had originally been measured with the G1 ORA. The difference in CH between the devices in both groups was approximately 0.5 mmHg. Although this difference is statistically significant, it is important to consider whether this is a clinically significant difference. Clinical studies on glaucoma patients and their controls suggest that a CH value of 10 mmHg is average, 9.0-9.5 mmHg is suspicious for glaucoma conversion or progression, and <8.0 mmHg is a risk factor for conversion or progression (Shah et al., 2007; Susanna et al., 2018; Wells et al., 2008). According to these values, a 0.5 mmHg difference in CH could be considered as being clinically significant, as changes of CH by 0.5 mmHg may change the risk category into which a patient is placed. Moreover, a study by Susanna et al. showed that glaucoma suspects who converted to glaucoma had a mean CH of 9.5 ± 1.5 mmHg, and glaucoma suspects who did not convert to glaucoma had a mean CH of 10.2 ± 1.5 mmHg. The mean difference in CH between the two groups in the Susanna study was 0.7 mmHg, which is within 0.2 mmHg of the difference found in this study. Thus, the difference in CH found between devices in

this study may have impact on clinical decision making. Although CH is not the only factor considered when deciding to begin or alter glaucoma treatment, CH can influence these decisions and can impact how closely a clinician chooses to follow a patient at risk for glaucoma conversion or progression.

In summary, differences in biomechanical parameters between the G1 and G3 ORA indicate that it is important to consider the generation of device used when interpreting results in the clinic and from studies of ocular biomechanics. Results of a study using the G1 ORA should not be compared directly with those of a study that utilized the G3 ORA, specifically when parameters being compared include CH and waveform parameters. On the other hand, IOPcc and IOPg results could be compared between studies that utilize differing devices, as the results of this study indicated that these values do not differ between the devices. Furthermore, it is important for researchers to indicate which generation of the ORA device was used in a study, as the G1 and G3 devices are not always interchangeable.

Differences in IOP and Biomechanical Parameters Between Case and Control Cohorts as Measured by G1 ORA and G3 ORA

This study also demonstrated differences in IOP and biomechanical parameters between eyes with keratoconus and normal eyes. Normal eyes had significantly greater IOPcc, IOPg, CH, WS, p1area, p2area, h1, h2, and KMI than the case cohort when measured with the G1 ORA. There were no statistically significant differences in w1 and w2 between the two cohorts. These results were similar when using the G3 ORA; normal eyes had significantly greater IOPcc, IOPg, CH, WS, p1area, p2area, h1, h2, w1 and KMI

than the case cohort. The only parameter that did not significantly differ between the two cohorts was w_2 .

These results can be interpreted to suggest that the normal eyes were stiffer than the eyes with keratoconus. Normal eyes had higher h_1 , h_2 , p_1 area, and p_2 area, which, as explained previously, correlates with a broader applanation area, and thus a stiffer cornea. A study by Luz et al. also demonstrated higher h_1 , h_2 , p_1 area, and p_2 area in normal eyes compared to keratoconic eyes (Luz et al., 2013). The keratoconic cohort's lower h_1 , h_2 , p_1 area, and p_2 area in the keratoconus cohort imply that those eyes had a smaller applanation area, and thus a weaker cornea.

It is widely accepted that corneal tissue weakens in keratoconus. Uniaxial strip testing of donor tissues first revealed diminished tensile strength in keratoconic corneas compared to healthy corneas (Andreassen et al., 1980), and now there is good evidence for elastic deterioration of the cornea in the eyes of patients living with keratoconus (Bak-Nielsen et al., 2014; Tian et al., 2014; Yang et al., 2019). One might interpret these results as evidence that the entire cornea weakens in keratoconus, but this interpretation is flawed since these methods were unable to assess asymmetry. Finite element modeling has identified loss of tissue stiffness, which is localized to a concentric area around the location of the cone, as a contributor to keratoconus progression (Falgayrettes et al., 2023). Specifically, Falgayrettes et al. found that weakening corneal stromal tissue of a previously healthy cornea button over the whole cornea did not result in cone formation, but weakening of stromal tissue in a focal inferocentral portion of the corneal button did result in cone formation. Moreover, several groups have used Brillouin microscopy, a form of non-destructive optical elastography (Prevedel et al., 2019), to demonstrate focal,

not global, weakness in keratoconus that is associated with local corneal thinning and steepening (Scarcelli et al., 2015; Scarcelli et al., 2014; Shao et al., 2019). In other words, there is an asymmetry in corneal biomechanical parameters, relative tissue weakness adjacent to relative tissue strength, which is typically not accounted for in the clinical assessment of keratoconus, as most methods of measuring corneal biomechanics in vivo in a clinical setting, including the ORA, are not capable of assessing asymmetry.

The results of this study agree with past studies that have shown IOPg and IOPcc are higher in normal eyes compared to keratoconic eyes when measured with the ORA, (Alipour et al., 2021; Luz et al., 2013). This difference may be due to the case group having thinner corneas and lower CH compared to the control group (Alipour et al., 2021; Shah & Laiquzzaman, 2009; Shah et al., 2007). Higher WS in the control group may indicate that normal eyes produce a more repeatable output waveform than keratoconic eyes. Higher CH in the control group agrees with past studies that have demonstrated lower CH in keratoconic eyes compared to normal eyes (Fontes et al., 2010; Luz et al., 2013; Ortiz et al., 2007; Shah et al., 2007). However, due to significant overlap in the distribution of CH between the two groups, it is not a good differentiator between the groups. As an alternative to CH, assessment of the characteristics of the ORA waveform itself may provide better sensitivity to detect keratoconus and other ectasias; the KMI metric aims to address this limitation using specific waveform parameters.

Ability of KMI to Differentiate between Cases and Controls with G1 ORA and G3 ORA

The second purpose of this study was to evaluate the ability of the G3 ORA to use the KMI metric, which was developed on and for the G1 device, to identify eyes with

keratoconus. In this study, KMI was higher in the control group, which agrees with past studies that have also compared KMI in normal and keratoconic eyes (Labiris et al., 2013). In the G1 dataset, KMI was able to differentiate keratoconic eyes from normal eyes with an area under the ROC curve of 0.86. In the G3 dataset, KMI was able to differentiate keratoconic eyes from normal eyes with an area under the ROC curve of 0.88. Although the G3 ORA was more sensitive and specific at differentiating the cohorts than the G1, the difference was small and thus likely not meaningful. As a result, it can be concluded that the KMI performs similarly between the G1 and G3 ORA in identifying keratoconic eyes.

Although the KMI developed on the G1 device has shown relatively high sensitivity and specificity for identifying keratoconus, it is important to consider the impact or severity of the disease in question when considering whether or not a test can identify it successfully. For example, a false negative result for a test that attempts to detect a disease with severe health implications is more consequential to health-related quality of life than a false negative result from a test attempting to identify a less consequential disease. Keratoconus, when not diagnosed in a timely manner, can result in vision loss, can impart significant cost burden (Chan et al., 2020), and can reduce quality of life (Al Zabadi et al., 2023). Therefore, while the predictive value of the KMI shown by these results may be considered relatively good, a higher predictive value is desirable in order to enhance the utility of KMI in clinical practice. As the biomechanical parameters measured by the G3 ORA differ significantly from those measured by the G1 ORA, there is a need to update and optimize the existing KMI for the G3 device. The original KMI was developed using univariate t-tests that compared differences in the

mean values of each waveform parameter measured with G1 ORA between a population of normal eyes and a population of keratoconic eyes. The seven waveform parameters with the largest differences between the cohorts were identified and combined into a single metric, KMI. Because this study shows that the G1 and G3 ORA differ in their assessment of biomechanical parameters, this same development process can be applied to G3 ORA data to identify parameters that vary most between the two cohorts. The “new” KMI has the potential to be more sensitive and specific than the “old” KMI metric. This task will require development and independent validation on large and diverse datasets in order to maximize the robustness of the resulting algorithm.

Cone Location

The third purpose of this study was to investigate whether cone location influences the ORA-measured biomechanical parameters of the cornea in keratoconus. Our hypothesis was confirmed: central cones exhibit different biomechanical responses to the air puff in comparison to peripheral cones. Parameters WS, p1area, p2area, h1, and h2 were significantly different between the central cones and the peripheral cones, regardless of whether axial or tangential topography was utilized to identify the cone. Moreover, there were statistically significant moderate-to-weak associations between cone location and WS, p1area, p2area, h1, and h2 for both curvature algorithms. As mentioned previously, past studies have demonstrated that weakening of the cornea in keratoconus is focal, not global in nature. In other words, there is tissue weakness adjacent to relative tissue strength (Falgayrettes et al., 2023; Scarcelli et al., 2015; Scarcelli et al., 2014; Shao et al., 2019). The impact that cone location has on the assessment of biomechanical

parameters demonstrated by this study provides further evidence that keratoconus is due to a focal weakening of corneal tissue, rather than global weakening of tissue.

These results suggest that cone location should be considered when interpreting biomechanical measurements in eyes with keratoconus. As described previously, the two states of applanation are represented by the two peaks on the output waveform graphing the cornea's response to the air puff, as the y-axis of the output waveform represents number of photons detected by the photon sensor. A large area of applanation allows many photons to reflect into the sensor, resulting in a high peak, and a small area of applanation allows relatively few photons to align with the sensor, resulting in a lower peak. The central cone cohort had a smaller p1 area and smaller p2 area than the peripheral cone cohort. These differences were driven by the height of the peaks, and not the widths, as h1 and h2 were significantly smaller in the central cone cohorts, and there were no inter-cohort differences in w1 and w2. These outcomes indicate that the first and second applanation areas were larger for the peripheral-cone cohort than for the central cone-cohort and can be interpreted as strongly suggesting that the peripheral-cone cohort had stiffer central corneas than the central-cone cohort. As explained previously in the analogy of two hollow spheres, if one were to push on the two spheres, the stiffer material of Sphere A results in a broad shallow indentation, while the more compliant material of Sphere B would result in a deep but narrow indentation. In the same way, an ORA air puff delivered to a relatively stiff central cornea (e.g., peripheral keratoconus) would elicit a boarder applanation area, and therefore a higher waveform peak (Fig. 8a), than an ORA air puff delivered to a compliant central cornea (e.g., central keratoconus; Fig. 8b).

The results of this study also demonstrate that cone location should be considered when using biomechanical assessment to supplement keratoconus detection, as central cones and peripheral cones may produce differing waveform outputs when using the G3 ORA. Figure 9 compares two different corneas' responses to the air puff, one a normal cornea's response (9a), and the second a keratoconic cornea with a peripheral cone's response (9b). These waveforms are very similar due to the relative stiffness of the central cornea in both eyes, and therefore an eye with early peripheral keratoconus may be mistaken as being normal, or stiffer globally without detecting the peripheral focal weakness. Mistaking peripheral keratoconus as a normal eye may delay timely diagnosis and management of disease or result in inaccurate assessment of risk before refractive surgery when utilizing biomechanical methods to detect keratoconus. Corneal ectasia following LASIK surgery has been attributed to removal of excess tissue during surgery, leaving a less than sufficient residual corneal stromal bed, or possible presence of sub-clinical keratoconus that manifests more severely after compromise of the structural integrity of the cornea following LASIK (Moshirfar et al., 2021). Therefore, sub-clinical keratoconus detection is important in screening before refractive surgery, and clinicians must be aware of the similarities in waveform morphology between normal eyes and eyes with peripheral cones if using a biomechanical approach during screening.

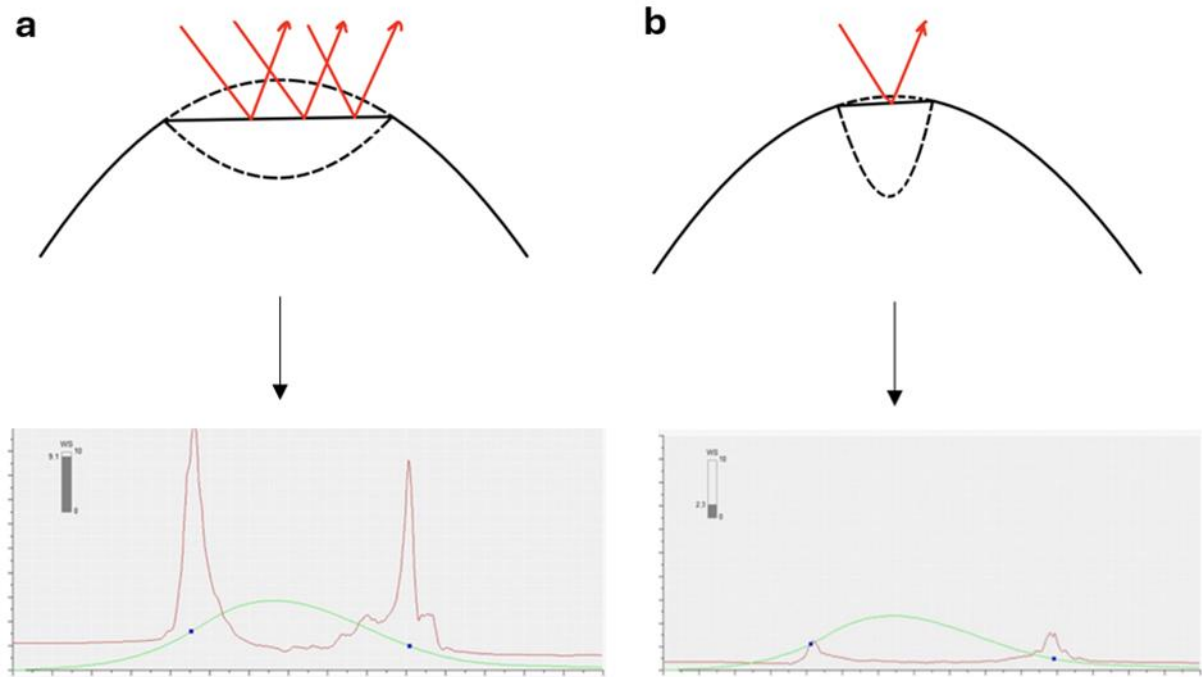


Figure 8. Schematic representation of the effect that corneal stiffness has on reflected photons. A stiff central cornea, (a) such as with a peripheral cone, results in broader area of appplanation, and thus more photons reflected into the photodetector of the ORA, producing higher peaks on the waveform, than a compliant central cornea (b), such as with a central cone, which has a narrow area of appplanation, producing lower peaks on the waveform.

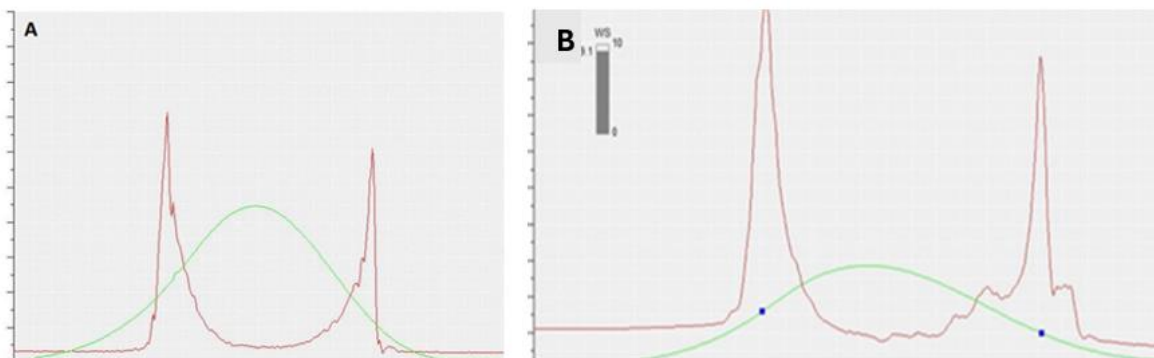


Figure 9. Sample output waveforms of A) a normal eye's response to the air puff and B) a keratoconic eye with a peripheral cone's response to the air puff.

ORA Agreement with Past Evidence of Cone Location Impact on Biomechanical Parameters

This study is the first to investigate the differences in biomechanical parameters between eyes with peripheral cones and eyes with central cones using the ORA. Another study has used other technology to assess differences in biomechanics between central and peripheral cones. Cornea Visualization with Scheimpflug Technology (Corvis ST; Oculus, Wetzlar, Germany) tonometer uses a high-speed Scheimpflug camera to capture images of air-puff-induced corneal deformation, which are then analyzed to produce elastic biomechanical parameters of the living human eye (Ambrosio et al., 2013). Many studies have demonstrated elastic weakening of the keratoconic cornea using the Corvis ST (Bak-Nielsen et al., 2014; Sedaghat et al., 2021; Tian et al., 2014; Yang et al., 2019), and the device's biomechanical index, which is a metric that comprises an array of elastic biomechanical parameters, is able to differentiate corneas with keratoconus from healthy corneas with high accuracy (Vinciguerra et al., 2016). Pertinent to the present study, Bruner and colleagues used the Corvis ST to measure increasing corneal stiffness with increasing cone eccentricity in keratoconus by analyzing elastic outcome measures: stiffness parameter at first applanation, stiffness parameter at highest concavity, deformation amplitude ratio, and integrated inverse radius (Bruner C, 2022). These results on the Corvis ST align with the results of this study on the ORA and offer cross-device evidence for the focal nature of the biomechanical weakening in keratoconus.

Utilization of the ORA in Research and Clinic

The ORA remains a useful tool in the assessment of ocular biomechanics. First, given that ORA received approval from the Food and Drug Administration nearly two decades ago, it is inexpensive in comparison to other biomechanics assessment technology like Corvis ST, and is more common in primary eye care clinics, where keratoconus is often detected, than the Corvis ST, which most often is found in specialty cornea clinics. The ORA can also be utilized in the assessment of glaucoma risk, as ORA can provide CH, which is associated with glaucoma progression (Medeiros et al., 2013; Susanna et al., 2018). Second, the ORA has the potential to measure both the viscoelastic properties of the eye (e.g., CH) and the elastic parameters of the eye, the latter through analysis of the morphology of the ORA waveform (Qin et al., 2019). The Corvis ST can only quantify the elastic parameters of the eye at the current time. Finally, for the purpose of this study, the delivery of an air puff to the central cornea allows for the quantification of the effect of cone location on biomechanical parameters in patients with keratoconus. Although the ORA and the Corvis ST vary in their assessment of corneal deformation in response to a central air puff, the underlying principle that is supported here – namely that of asymmetry in corneal biomechanical parameters in keratoconus – is generalizable across both of them.

Beyond informing our knowledge of corneal weakness in keratoconus, regional variability of the biomechanical parameters has practical implications. First, future clinical studies on corneal biomechanics in keratoconus may consider cone location during study design and during data analysis. A study cohort with a disproportionate number of central cones may skew results toward greater corneal compliance in the

disease, compared against a cohort with a disproportionate number of peripheral cones, which may skew results toward greater corneal stiffness. Furthermore, a study cohort with an overrepresentation either of central cones or of peripheral cones would likely not be generalizable to a broader population of patients with keratoconus. Rather, a keratoconus study with a mix of central cones and peripheral cones will maximize its applicability. In the clinic, a patient with a peripheral cone may exhibit greater corneal stiffness than a patient with a central cone. In a case of manifest keratoconus, this difference would not influence clinical decision making. However, if the patient had early-stage peripheral keratoconus – where there was no clear steepening indicated on the corneal topography map, there were no signs of the disease on slit-lamp biomicroscopy, and notable vision loss had not yet manifested – measurement of biomechanical parameters, as a supplemental means of disease detection, might lead the clinician to conclude that the cornea was relatively stiffer globally without detecting the focal peripheral weakness, potentially delaying timely diagnosis and management.

Influence of Topography Algorithm

In this population of participants with keratoconus, cone location varied based on topography algorithm. There were more central cones in the tangential topography maps than in the axial topography maps. This difference is expected since the axial curvature algorithm is the mathematical average of the tangential curvature algorithm, so the cone will be represented more peripherally in an axial map than a tangential map. This difference is also consistent with the literature, which reports varying cone location for different map types and for different instruments (Sedaghat et al., 2021; Steinwender

et al., 2022). It did not have a marked effect on the results, however, as there were significant differences in p1area, p2area, h1, and h2 between the peripheral-cone and central-cone cohorts for both types of curvature. There were also significant associations between cone location and those waveform parameters for both topography curvature algorithms, demonstrating that the further the cone is from the center of the cornea, the larger the magnitude of a given stiffness parameter.

Study Limitations

This study has several limitations. First, the sample size was small, and a difference in CH based on cone location was unable to be detected. This is likely because the cornea is not the only ocular structure that influences the ORA waveform. There is evidence that the sclera also contributes, as CH and other waveform parameters of the second peak of the waveform are reduced in eyes that have received a scleral buckle for the repair of retinal detachment, compared to fellow eyes (Taroni et al., 2020). Thus, CH can be interpreted as ocular hysteresis, rather than as corneal, alone. Beyond the impact that the sample size may have had on the outcomes, lack of difference in CH between the groups makes sense for this reason. Second, corneal pachymetry values were not considered in analysis. In keratoconus, corneal thinning and corneal steepening occur in conjunction, and it is thinning which drives a steepening response (Roberts & Dupps, 2014), so it is likely that central corneal thickness varied between the central-cone and the peripheral cone cohorts. According to the biomechanical cycle of decompensation in ectasia (Roberts & Dupps, 2014) both focal thinning and focal steepening result from a focally reduced modulus of elasticity, for which *in vivo* evidence is provided in this

study. Since focal thinning and focal steepening are so intimately connected in keratoconus and other ectasias, only measuring focal steepening, in the form of Cspot, was likely sufficient to study the focal nature of corneal decompensation in keratoconus. Third, it is possible that the control group included eyes with subclinical keratoconus, which could confound the differences found between the control group and case group as measured with both ORA devices. Finally, this study was cross-sectional and therefore could not assess how the biomechanical parameters of eyes in the study changed with time. Future studies should consider a longitudinal approach to characterize corneal biomechanical parameters to improve risk profiling for both the detection of keratoconus and for its management.

Conclusions

This study demonstrated that the air jet delivery and applanation detection system hardware changes incorporated in the G3 ORA did affect quantification of biomechanical waveform parameters, but IOPg and IOPcc remained relatively unaltered. Thus, comparisons between IOP measurements can be made in confidence between the two devices, but CH and other waveform parameter comparisons cannot be directly made. These differences in biomechanical waveform parameters between the G1 and G3 ORA indicate that it is important to consider the generation of device used when interpreting results in the clinic and from studies of ocular biomechanics. Additionally, this study agreed with previous studies that normal eyes produce stiffer deformation responses to the air puff compared to keratoconic eyes.

This study also evaluated the ability of KMI to differentiate keratoconic eyes from normal eyes. KMI performs similarly when used with input data from either G1 ORA or G3 ORA. The G3 ORA measured biomechanical parameters differently from the G1 ORA, so there may be parameters that differ more between the case and control cohorts than the parameters originally included in the development of KMI. Therefore, future studies in this line of work should aim to optimize the existing KMI for the G3 ORA to increase its ability to identify keratoconus.

This study also demonstrated that cone location in keratoconus influences the measurement of biomechanical parameters of the cornea when assessed with the ORA. Specifically, ORA waveform parameters p1area, p2area, h1, and h2 were significantly lower in the central-cone cohort than in the peripheral cone cohort, both for when cone location was determined with axial topography and for when cone location was determined with tangential topography. These results can be interpreted as suggesting that participants with peripheral cones had stiffer central corneas than participants with central cones. This interpretation is consistent with previous works that suggest localized lamellar disorganization and focal corneal weakening in the disease. It is strongly recommended that researchers and clinicians consider cone location when analyzing biomechanical data.

References

- Al Zabadi, H., Shehadeh, M., Amro, L., Ghattass, N., & Taha, I. (2023). Vision-related quality of life among patients with keratoconus: a cross sectional study. *Front Med (Lausanne)*, *10*, 1208911. <https://doi.org/10.3389/fmed.2023.1208911>
- Alipour, F., Hassanpoor, N., Letafatnejad, M., Beheshtnejad, A. H., & Mohammadi, S. F. (2021). Tonometry by Ocular Response Analyzer in Keratoconic and Warpage Eyes in Comparison with Normal Eyes. *J Curr Ophthalmol*, *33*(2), 118-123. https://doi.org/10.4103/JOCO.JOCO_147_20
- Ambrosio, R., Jr., Valbon, B. F., Faria-Correia, F., Ramos, I., & Luz, A. (2013). Scheimpflug imaging for laser refractive surgery. *Curr Opin Ophthalmol*, *24*(4), 310-320. <https://doi.org/10.1097/ICU.0b013e3283622a94>
- Andreassen, T. T., Simonsen, A. H., & Oxlund, H. (1980). Biomechanical properties of keratoconus and normal corneas. *Exp Eye Res*, *31*(4), 435-441. [https://doi.org/10.1016/s0014-4835\(80\)80027-3](https://doi.org/10.1016/s0014-4835(80)80027-3)
- Ashwin, P. T., & McDonnell, P. J. (2010). Collagen cross-linkage: a comprehensive review and directions for future research. *Br J Ophthalmol*, *94*(8), 965-970. <https://doi.org/10.1136/bjo.2009.164228>
- Asimakis, P., & Kirkness, C. M. (1996). Storage of donor corneas, surgery, outcome, and complications of penetrating keratoplasty. *Curr Opin Ophthalmol*, *7*(4), 35-40. <https://doi.org/10.1097/00055735-199608000-00007>
- Bak-Nielsen, S., Pedersen, I. B., Ivarsen, A., & Hjortdal, J. (2014). Dynamic Scheimpflug-based assessment of keratoconus and the effects of corneal cross-linking. *J Refract Surg*, *30*(6), 408-414. <https://doi.org/10.3928/1081597X-20140513-02>
- Borderie, V. M., Georgeon, C., Sandali, O., & Bouheraoua, N. (2023). Long-term outcomes of deep anterior lamellar versus penetrating keratoplasty for keratoconus. *Br J Ophthalmol*, *108*(1), 10-16. <https://doi.org/10.1136/bjo-2023-324230>
- Borgardt, K., Menzel-Severing, J., Fischinger, I., Geerling, G., & Seiler, T. G. (2023). Innovations in Corneal Crosslinking. *Curr Eye Res*, *48*(2), 144-151. <https://doi.org/10.1080/02713683.2022.2146725>
- Bron, A. J., & Rabinowitz, Y. S. (1996). Corneal dystrophies and keratoconus. *Curr Opin Ophthalmol*, *7*(4), 71-82. <https://doi.org/10.1097/00055735-199608000-00013>
- Bruner C, M. A., Roberts CJ. . (2022). Cone location and corneal stiffness in keratoconus. . *Invest Ophthalmol Vis Sci.*, *63*.
- Bureau, J., Pouliquen, Y., & Lorans, G. (1993). [Fibrocyte reaction to interleukin 1 stimulation in keratoconus. Original title: Fibrocyte response to interleukin 1 stimulation in keratoconus]. *Klin Monbl Augenheilkd*, *203*(4), 269-274.

- <https://doi.org/10.1055/s-2008-1045679> (Fibrozytenreaktion auf Interleukin-1-stimulation bei Keratokonus. Originaltitel: Fibrocyte response to interleukin 1 stimulation in keratoconus.)
- Chan, E., Baird, P. N., Vogrin, S., Sundararajan, V., Daniell, M. D., & Sahebjada, S. (2020). Economic impact of keratoconus using a health expenditure questionnaire: A patient perspective. *Clin Exp Ophthalmol*, 48(3), 287-300. <https://doi.org/10.1111/ceo.13704>
- Colin, J., Cochener, B., Savary, G., & Malet, F. (2000). Correcting keratoconus with intracorneal rings. *J Cataract Refract Surg*, 26(8), 1117-1122. [https://doi.org/10.1016/s0886-3350\(00\)00451-x](https://doi.org/10.1016/s0886-3350(00)00451-x)
- Cristina Kenney, M., & Brown, D. J. (2003). The cascade hypothesis of keratoconus. *Cont Lens Anterior Eye*, 26(3), 139-146. [https://doi.org/10.1016/S1367-0484\(03\)00022-5](https://doi.org/10.1016/S1367-0484(03)00022-5)
- Du, X. L., Chen, M., & Xie, L. X. (2015). Correlation of basic indicators with stages of keratoconus assessed by Pentacam tomography. *Int J Ophthalmol*, 8(6), 1136-1140. <https://doi.org/10.3980/j.issn.2222-3959.2015.06.10>
- Eliasy, A., Abass, A., Lopes, B. T., Vinciguerra, R., Zhang, H., Vinciguerra, P., Ambrosio, R., Jr., Roberts, C. J., & Elsheikh, A. (2020). Characterization of cone size and centre in keratoconic corneas. *J R Soc Interface*, 17(169), 20200271. <https://doi.org/10.1098/rsif.2020.0271>
- Elsheikh, A., Wang, D., Brown, M., Rama, P., Campanelli, M., & Pye, D. (2007). Assessment of corneal biomechanical properties and their variation with age. *Curr Eye Res*, 32(1), 11-19. <https://doi.org/10.1080/02713680601077145>
- Falgayrettes, N., Patoor, E., Cleymand, F., Zevering, Y., & Perone, J. M. (2023). Biomechanics of keratoconus: Two numerical studies. *PLoS One*, 18(2), e0278455. <https://doi.org/10.1371/journal.pone.0278455>
- Faria-Correia, F. (2012). Topometric and Tomographic Indices for the Diagnosis of Keratoconus. *International Journal of Keratoconus and Ectatic Corneal Diseases*. <https://doi.org/10.5005/jp-journals-10025-1018>
- Fernandez, J., Rodriguez-Vallejo, M., Martinez, J., Tauste, A., & Pinero, D. P. (2016). Corneal Thickness After SMILE Affects Scheimpflug-based Dynamic Tonometry. *J Refract Surg*, 32(12), 821-828. <https://doi.org/10.3928/1081597X-20160816-02>
- Fontes, B. M., Ambrosio, R., Jr., Jardim, D., Velarde, G. C., & Nose, W. (2010). Corneal biomechanical metrics and anterior segment parameters in mild keratoconus. *Ophthalmology*, 117(4), 673-679. <https://doi.org/10.1016/j.ophtha.2009.09.023>
- Fortman, M. M., Mahmoud, A. M., Roberts, C. J., & Yuhas, P. T. (2023). Intraocular pressure and biomechanical parameters measured with two generations of dynamic bidirectional air-puff tonometers in subjects with keratoconus and in healthy controls. *Invest. Ophthalmol Vis. Sci*, 64(8), 1701.
- Franco, J., White, C. A., & Kruh, J. N. (2020). Analysis of Compensatory Corneal Epithelial Thickness Changes in Keratoconus Using Corneal Tomography. *Cornea*, 39(3), 298-302. <https://doi.org/10.1097/ICO.0000000000002156>

- Gasset, A. R., Houde, W. L., & Garcia-Bengochea, M. (1978). Hard contact lens wear as an environmental risk in keratoconus. *Am J Ophthalmol*, 85(3), 339-341. [https://doi.org/10.1016/s0002-9394\(14\)77725-6](https://doi.org/10.1016/s0002-9394(14)77725-6)
- Godefrooij, D. A., de Wit, G. A., Uiterwaal, C. S., Imhof, S. M., & Wisse, R. P. (2017). Age-specific Incidence and Prevalence of Keratoconus: A Nationwide Registration Study. *Am J Ophthalmol*, 175, 169-172. <https://doi.org/10.1016/j.ajo.2016.12.015>
- Gomes, J. A., Rapuano, C. J., Belin, M. W., Ambrosio, R., Jr., Group of Panelists for the Global Delphi Panel of, K., & Ectatic, D. (2015). Global Consensus on Keratoconus Diagnosis. *Cornea*, 34(12), e38-39. <https://doi.org/10.1097/ICO.0000000000000623>
- Gonzalez, V., & McDonnell, P. J. (1992). Computer-assisted corneal topography in parents of patients with keratoconus. *Arch Ophthalmol*, 110(10), 1413-1414. <https://doi.org/10.1001/archophth.1992.01080220074024>
- Gordon-Shaag, A., Millodot, M., Shneor, E., & Liu, Y. (2015). The genetic and environmental factors for keratoconus. *Biomed Res Int*, 2015, 795738. <https://doi.org/10.1155/2015/795738>
- Greenstein, S. A., Fry, K. L., & Hersh, P. S. (2012). Effect of topographic cone location on outcomes of corneal collagen cross-linking for keratoconus and corneal ectasia. *J Refract Surg*, 28(6), 397-405. <https://doi.org/10.3928/1081597X-20120518-02>
- Hafezi, F., Kling, S., Gilardoni, F., Hafezi, N., Hillen, M., Abrishamchi, R., Gomes, J. A. P., Mazzotta, C., Randleman, J. B., & Torres-Netto, E. A. (2021). Individualized Corneal Cross-linking With Riboflavin and UV-A in Ultrathin Corneas: The Sub400 Protocol. *Am J Ophthalmol*, 224, 133-142. <https://doi.org/10.1016/j.ajo.2020.12.011>
- Henein, C., & Nanavaty, M. A. (2017). Systematic review comparing penetrating keratoplasty and deep anterior lamellar keratoplasty for management of keratoconus. *Cont Lens Anterior Eye*, 40(1), 3-14. <https://doi.org/10.1016/j.clae.2016.10.001>
- Hersh, P. S., Stulting, R. D., Muller, D., Durrie, D. S., Rajpal, R. K., & United States Crosslinking Study, G. (2017). United States Multicenter Clinical Trial of Corneal Collagen Crosslinking for Keratoconus Treatment. *Ophthalmology*, 124(9), 1259-1270. <https://doi.org/10.1016/j.ophtha.2017.03.052>
- Kaushik, S., & Pandav, S. S. (2012). Ocular Response Analyzer. *J Curr Glaucoma Pract*, 6(1), 17-19. <https://doi.org/10.5005/jp-journals-10008-1103>
- Kennedy, R. H., Bourne, W. M., & Dyer, J. A. (1986). A 48-year clinical and epidemiologic study of keratoconus. *Am J Ophthalmol*, 101(3), 267-273. [https://doi.org/10.1016/0002-9394\(86\)90817-2](https://doi.org/10.1016/0002-9394(86)90817-2)
- Krachmer, J. H., Feder, R. S., & Belin, M. W. (1984). Keratoconus and related noninflammatory corneal thinning disorders. *Surv Ophthalmol*, 28(4), 293-322. [https://doi.org/10.1016/0039-6257\(84\)90094-8](https://doi.org/10.1016/0039-6257(84)90094-8)
- Kreps, E. O., Claerhout, I., & Koppen, C. (2021). Diagnostic patterns in keratoconus. *Cont Lens Anterior Eye*, 44(3), 101333. <https://doi.org/10.1016/j.clae.2020.05.002>

- Labiris, G., Gatzoufas, Z., Sideroudi, H., Giarmoukakis, A., Kozobolis, V., & Seitz, B. (2013). Biomechanical diagnosis of keratoconus: evaluation of the keratoconus match index and the keratoconus match probability. *Acta Ophthalmol*, 91(4), e258-262. <https://doi.org/10.1111/aos.12056>
- Labiris, G., Giarmoukakis, A., Sideroudi, H., Song, X., Kozobolis, V., Seitz, B., & Gatzoufas, Z. (2014). Diagnostic capacity of biomechanical indices from a dynamic bidirectional applanation device in pellucid marginal degeneration. *J Cataract Refract Surg*, 40(6), 1006-1012. <https://doi.org/10.1016/j.jcrs.2014.03.018>
- Luce, D., & Taylor, D. . (2016). Ocular Response Analyzer In C. J. R. J. Liu (Ed.), *Corneal Biomechanics: From Theory to Practice*.
- Luz, A., Fontes, B. M., Lopes, B., Ramos, I., Schor, P., & Ambrosio, R., Jr. (2013). ORA waveform-derived biomechanical parameters to distinguish normal from keratoconic eyes. *Arq Bras Oftalmol*, 76(2), 111-117. <https://doi.org/10.1590/s0004-27492013000200011>
- Mahmoud, A. M., Roberts, C. J., Lembach, R. G., Twa, M. D., Herderick, E. E., McMahan, T. T., & Group, C. S. (2008). CLMI: the cone location and magnitude index. *Cornea*, 27(4), 480-487. <https://doi.org/10.1097/ICO.0b013e31816485d3>
- Marcos, S. K. L. R. A. P.-E. J. M.-L. S. (2010). Corneal Biomechanical Changes after Collagen Cross-Linking from Porcine Eye Inflation Experiments. *Investigative Ophthalmology & Visual Science*, 51. <https://doi.org/https://doi.org/10.1167/iovs.09-4536>
- Martin, R. (2018). Cornea and anterior eye assessment with placido-disc keratometry, slit scanning evaluation topography and scheimpflug imaging tomography. *Indian J Ophthalmol*, 66(3), 360-366. https://doi.org/10.4103/ijo.IJO_850_17
- Medeiros, F. A., Meira-Freitas, D., Lisboa, R., Kuang, T. M., Zangwill, L. M., & Weinreb, R. N. (2013). Corneal hysteresis as a risk factor for glaucoma progression: a prospective longitudinal study. *Ophthalmology*, 120(8), 1533-1540. <https://doi.org/10.1016/j.ophtha.2013.01.032>
- Meek, K. M., Tuft, S. J., Huang, Y., Gill, P. S., Hayes, S., Newton, R. H., & Bron, A. J. (2005). Changes in collagen orientation and distribution in keratoconus corneas. *Invest Ophthalmol Vis Sci*, 46(6), 1948-1956. <https://doi.org/10.1167/iovs.04-1253>
- Mimouni, M., Sorkin, N., Trinh, T., Group, K. C. S., Hatch, W., & Singal, N. (2021). Central versus paracentral cone location and outcomes of accelerated cross-linking in keratoconus patients. *Eye (Lond)*, 35(12), 3311-3317. <https://doi.org/10.1038/s41433-021-01404-5>
- Moshirfar, M., Motlagh, M. N., Murri, M. S., Momeni-Moghaddam, H., Ronquillo, Y. C., & Hoopes, P. C. (2019). Galilei Corneal Tomography for Screening of Refractive Surgery Candidates: A Review of the Literature, Part II. *Med Hypothesis Discov Innov Ophthalmol*, 8(3), 204-218. <https://www.ncbi.nlm.nih.gov/pubmed/31598521>
- Naderan, M., Jahanrad, A., & Farjadnia, M. (2018). Ocular, corneal, and internal aberrations in eyes with keratoconus, forme fruste keratoconus, and healthy eyes. *Int Ophthalmol*, 38(4), 1565-1573. <https://doi.org/10.1007/s10792-017-0620-5>

- Nicula CA, B. A., Nicula D, Nicula AP, Horvath KU and Bolboacă SD. (2022). Performances of Corneal Topography and Tomography in the Diagnosis of Subclinical and Clinical Keratoconus. *Front. Med.*, 9. <https://doi.org/doi:10.3389/fmed.2022.904604>
- Ortiz, D., Pinero, D., Shabayek, M. H., Arnalich-Montiel, F., & Alio, J. L. (2007). Corneal biomechanical properties in normal, post-laser in situ keratomileusis, and keratoconic eyes. *J Cataract Refract Surg*, 33(8), 1371-1375. <https://doi.org/10.1016/j.jcrs.2007.04.021>
- Perry, H. D., Buxton, J. N., & Fine, B. S. (1980). Round and oval cones in keratoconus. *Ophthalmology*, 87(9), 905-909. [https://doi.org/10.1016/s0161-6420\(80\)35145-2](https://doi.org/10.1016/s0161-6420(80)35145-2)
- Prevedel, R., Diz-Munoz, A., Ruocco, G., & Antonacci, G. (2019). Brillouin microscopy: an emerging tool for mechanobiology. *Nat Methods*, 16(10), 969-977. <https://doi.org/10.1038/s41592-019-0543-3>
- Qin, X., Yu, M., Zhang, H., Chen, X., & Li, L. (2019). The Mechanical Interpretation of Ocular Response Analyzer Parameters. *Biomed Res Int*, 2019, 5701236. <https://doi.org/10.1155/2019/5701236>
- Rabinowitz, Y. S. (1998). Keratoconus. *Surv Ophthalmol*, 42(4), 297-319. [https://doi.org/10.1016/s0039-6257\(97\)00119-7](https://doi.org/10.1016/s0039-6257(97)00119-7)
- Randleman, J. B., Khandelwal, S. S., & Hafezi, F. (2015). Corneal cross-linking. *Surv Ophthalmol*, 60(6), 509-523. <https://doi.org/10.1016/j.survophthal.2015.04.002>
- Roberts, C. J., & Dupps, W. J., Jr. (2014). Biomechanics of corneal ectasia and biomechanical treatments. *J Cataract Refract Surg*, 40(6), 991-998. <https://doi.org/10.1016/j.jcrs.2014.04.013>
- Romero-Jimenez, M., Santodomingo-Rubido, J., & Wolffsohn, J. S. (2010). Keratoconus: a review. *Cont Lens Anterior Eye*, 33(4), 157-166; quiz 205. <https://doi.org/10.1016/j.clae.2010.04.006>
- Santodomingo-Rubido, J., Carracedo, G., Suzaki, A., Villa-Collar, C., Vincent, S. J., & Wolffsohn, J. S. (2022). Keratoconus: An updated review. *Cont Lens Anterior Eye*, 45(3), 101559. <https://doi.org/10.1016/j.clae.2021.101559>
- Scarcelli, G., Besner, S., Pineda, R., Kalout, P., & Yun, S. H. (2015). In vivo biomechanical mapping of normal and keratoconus corneas. *JAMA Ophthalmol*, 133(4), 480-482. <https://doi.org/10.1001/jamaophthalmol.2014.5641>
- Scarcelli, G., Besner, S., Pineda, R., & Yun, S. H. (2014). Biomechanical characterization of keratoconus corneas ex vivo with Brillouin microscopy. *Invest Ophthalmol Vis Sci*, 55(7), 4490-4495. <https://doi.org/10.1167/iovs.14-14450>
- Sedaghat, M. R., Momeni-Moghaddam, H., Azimi Khorasani, A., Belin, M. W., Monfared, N., Wolffsohn, J. S., Pakdel, M., Farrokh Ghat, M., & Hemmatian, Z. (2021). Comparison of Keratoconus Cone Location of Different Topo/tomographical Parameters. *Curr Eye Res*, 46(11), 1666-1672. <https://doi.org/10.1080/02713683.2021.1931343>
- Shah, S., & Laiquzzaman, M. (2009). Comparison of corneal biomechanics in pre and post-refractive surgery and keratoconic eyes by Ocular Response Analyser. *Cont Lens Anterior Eye*, 32(3), 129-132; quiz 151. <https://doi.org/10.1016/j.clae.2008.12.009>

- Shah, S., Laiquzzaman, M., Bhojwani, R., Mantry, S., & Cunliffe, I. (2007). Assessment of the biomechanical properties of the cornea with the ocular response analyzer in normal and keratoconic eyes. *Invest Ophthalmol Vis Sci*, 48(7), 3026-3031. <https://doi.org/10.1167/iovs.04-0694>
- Shao, P., Eltony, A. M., Seiler, T. G., Tavakol, B., Pineda, R., Koller, T., Seiler, T., & Yun, S. H. (2019). Spatially-resolved Brillouin spectroscopy reveals biomechanical abnormalities in mild to advanced keratoconus in vivo. *Sci Rep*, 9(1), 7467. <https://doi.org/10.1038/s41598-019-43811-5>
- Shetty, R., Nuijts, R. M., Nicholson, M., Sargod, K., Jayadev, C., Veluri, H., & Sinha Roy, A. (2015). Cone location-dependent outcomes after combined topography-guided photorefractive keratectomy and collagen cross-linking. *Am J Ophthalmol*, 159(3), 419-425 e412. <https://doi.org/10.1016/j.ajo.2014.11.020>
- Steinwender, G., Kollenc, A., Shajari, M., Sommer, M., Borenich, A., Horwath-Winter, J., Lindner, E., Woltsche, N., List, W., & Wedrich, A. (2022). Determining the center of a keratoconus: Comparison of different tomographic parameters and impact of disease severity. *Front Med (Lausanne)*, 9, 968318. <https://doi.org/10.3389/fmed.2022.968318>
- Susanna, C. N., Diniz-Filho, A., Daga, F. B., Susanna, B. N., Zhu, F., Ogata, N. G., & Medeiros, F. A. (2018). A Prospective Longitudinal Study to Investigate Corneal Hysteresis as a Risk Factor for Predicting Development of Glaucoma. *Am J Ophthalmol*, 187, 148-152. <https://doi.org/10.1016/j.ajo.2017.12.018>
- Taroni, L., Bernabei, F., Pellegrini, M., Roda, M., Toschi, P. G., Mahmoud, A. M., Schiavi, C., Giannaccare, G., & Roberts, C. J. (2020). Corneal Biomechanical Response Alteration After Scleral Buckling Surgery for Rhegmatogenous Retinal Detachment. *Am J Ophthalmol*, 217, 49-54. <https://doi.org/10.1016/j.ajo.2020.03.054>
- Tian, L., Huang, Y. F., Wang, L. Q., Bai, H., Wang, Q., Jiang, J. J., Wu, Y., & Gao, M. (2014). Corneal biomechanical assessment using corneal visualization scheimpflug technology in keratoconic and normal eyes. *J Ophthalmol*, 2014, 147516. <https://doi.org/10.1155/2014/147516>
- Vinciguerra, R., Ambrosio, R., Jr., Elsheikh, A., Roberts, C. J., Lopes, B., Morenghi, E., Azzolini, C., & Vinciguerra, P. (2016). Detection of Keratoconus With a New Biomechanical Index. *J Refract Surg*, 32(12), 803-810. <https://doi.org/10.3928/1081597X-20160629-01>
- Wang, Y., Rabinowitz, Y. S., Rotter, J. I., & Yang, H. (2000). Genetic epidemiological study of keratoconus: evidence for major gene determination. *Am J Med Genet*, 93(5), 403-409. <https://www.ncbi.nlm.nih.gov/pubmed/10951465>
- Wells, A. P., Garway-Heath, D. F., Poostchi, A., Wong, T., Chan, K. C., & Sachdev, N. (2008). Corneal hysteresis but not corneal thickness correlates with optic nerve surface compliance in glaucoma patients. *Invest Ophthalmol Vis Sci*, 49(8), 3262-3268. <https://doi.org/10.1167/iovs.07-1556>
- Wilson, S. E., He, Y. G., Weng, J., Li, Q., McDowall, A. W., Vital, M., & Chwang, E. L. (1996). Epithelial injury induces keratocyte apoptosis: hypothesized role for the interleukin-1 system in the modulation of corneal tissue organization and wound healing. *Exp Eye Res*, 62(4), 325-327. <https://doi.org/10.1006/exer.1996.0038>

- Wojcik, K. A., Kaminska, A., Blasiak, J., Szaflik, J., & Szaflik, J. P. (2013). Oxidative stress in the pathogenesis of keratoconus and Fuchs endothelial corneal dystrophy. *Int J Mol Sci*, *14*(9), 19294-19308. <https://doi.org/10.3390/ijms140919294>
- Yang, K., Xu, L., Fan, Q., Zhao, D., & Ren, S. (2019). Repeatability and comparison of new Corvis ST parameters in normal and keratoconus eyes. *Sci Rep*, *9*(1), 15379. <https://doi.org/10.1038/s41598-019-51502-4>
- Al Zabadi, H., Shehadeh, M., Amro, L., Ghattass, N., & Taha, I. (2023). Vision-related quality of life among patients with keratoconus: a cross sectional study. *Front Med (Lausanne)*, *10*, 1208911. <https://doi.org/10.3389/fmed.2023.1208911>
- Alipour, F., Hassanpoor, N., Letafatnejad, M., Beheshtnejad, A. H., & Mohammadi, S. F. (2021). Tonometry by Ocular Response Analyzer in Keratoconic and Warpage Eyes in Comparison with Normal Eyes. *J Curr Ophthalmol*, *33*(2), 118-123. https://doi.org/10.4103/JOCO.JOCO_147_20
- Ambrosio, R., Jr., Valbon, B. F., Faria-Correia, F., Ramos, I., & Luz, A. (2013). Scheimpflug imaging for laser refractive surgery. *Curr Opin Ophthalmol*, *24*(4), 310-320. <https://doi.org/10.1097/ICU.0b013e3283622a94>
- Andreassen, T. T., Simonsen, A. H., & Oxlund, H. (1980). Biomechanical properties of keratoconus and normal corneas. *Exp Eye Res*, *31*(4), 435-441. [https://doi.org/10.1016/s0014-4835\(80\)80027-3](https://doi.org/10.1016/s0014-4835(80)80027-3)
- Ashwin, P. T., & McDonnell, P. J. (2010). Collagen cross-linkage: a comprehensive review and directions for future research. *Br J Ophthalmol*, *94*(8), 965-970. <https://doi.org/10.1136/bjo.2009.164228>
- Asimakis, P., & Kirkness, C. M. (1996). Storage of donor corneas, surgery, outcome, and complications of penetrating keratoplasty. *Curr Opin Ophthalmol*, *7*(4), 35-40. <https://doi.org/10.1097/00055735-199608000-00007>
- Bak-Nielsen, S., Pedersen, I. B., Ivarsen, A., & Hjortdal, J. (2014). Dynamic Scheimpflug-based assessment of keratoconus and the effects of corneal cross-linking. *J Refract Surg*, *30*(6), 408-414. <https://doi.org/10.3928/1081597X-20140513-02>
- Borderie, V. M., Georgeon, C., Sandali, O., & Bouheraoua, N. (2023). Long-term outcomes of deep anterior lamellar versus penetrating keratoplasty for keratoconus. *Br J Ophthalmol*, *108*(1), 10-16. <https://doi.org/10.1136/bjo-2023-324230>
- Borgardt, K., Menzel-Severing, J., Fischinger, I., Geerling, G., & Seiler, T. G. (2023). Innovations in Corneal Crosslinking. *Curr Eye Res*, *48*(2), 144-151. <https://doi.org/10.1080/02713683.2022.2146725>
- Bron, A. J., & Rabinowitz, Y. S. (1996). Corneal dystrophies and keratoconus. *Curr Opin Ophthalmol*, *7*(4), 71-82. <https://doi.org/10.1097/00055735-199608000-00013>
- Bruner C, M. A., Roberts CJ. . (2022). Cone location and corneal stiffness in keratoconus. . *Invest Ophthalmol Vis Sci.*, *63*.
- Bureau, J., Pouliquen, Y., & Lorans, G. (1993). [Fibrocyte reaction to interleukin 1 stimulation in keratoconus. Original title: Fibrocyte response to interleukin 1 stimulation in keratoconus]. *Klin Monbl Augenheilkd*, *203*(4), 269-274. <https://doi.org/10.1055/s-2008-1045679> (Fibrozytenreaktion auf Interleukin-1-

- stimulation bei Keratokonus. Originaltitel: Fibrocyte response to interleukin 1 stimulation in keratoconus.)
- Chan, E., Baird, P. N., Vogrin, S., Sundararajan, V., Daniell, M. D., & Sahebjada, S. (2020). Economic impact of keratoconus using a health expenditure questionnaire: A patient perspective. *Clin Exp Ophthalmol*, 48(3), 287-300. <https://doi.org/10.1111/ceo.13704>
- Colin, J., Cochener, B., Savary, G., & Malet, F. (2000). Correcting keratoconus with intracorneal rings. *J Cataract Refract Surg*, 26(8), 1117-1122. [https://doi.org/10.1016/s0886-3350\(00\)00451-x](https://doi.org/10.1016/s0886-3350(00)00451-x)
- Cristina Kenney, M., & Brown, D. J. (2003). The cascade hypothesis of keratoconus. *Cont Lens Anterior Eye*, 26(3), 139-146. [https://doi.org/10.1016/S1367-0484\(03\)00022-5](https://doi.org/10.1016/S1367-0484(03)00022-5)
- Du, X. L., Chen, M., & Xie, L. X. (2015). Correlation of basic indicators with stages of keratoconus assessed by Pentacam tomography. *Int J Ophthalmol*, 8(6), 1136-1140. <https://doi.org/10.3980/j.issn.2222-3959.2015.06.10>
- Eliasy, A., Abass, A., Lopes, B. T., Vinciguerra, R., Zhang, H., Vinciguerra, P., Ambrosio, R., Jr., Roberts, C. J., & Elsheikh, A. (2020). Characterization of cone size and centre in keratoconic corneas. *J R Soc Interface*, 17(169), 20200271. <https://doi.org/10.1098/rsif.2020.0271>
- Elsheikh, A., Wang, D., Brown, M., Rama, P., Campanelli, M., & Pye, D. (2007). Assessment of corneal biomechanical properties and their variation with age. *Curr Eye Res*, 32(1), 11-19. <https://doi.org/10.1080/02713680601077145>
- Falgayrettes, N., Patoor, E., Cleymand, F., Zevering, Y., & Perone, J. M. (2023). Biomechanics of keratoconus: Two numerical studies. *PLoS One*, 18(2), e0278455. <https://doi.org/10.1371/journal.pone.0278455>
- Faria-Correia, F. (2012). Topometric and Tomographic Indices for the Diagnosis of Keratoconus. *International Journal of Keratoconus and Ectatic Corneal Diseases*. <https://doi.org/10.5005/jp-journals-10025-1018>
- Fernandez, J., Rodriguez-Vallejo, M., Martinez, J., Tauste, A., & Pinero, D. P. (2016). Corneal Thickness After SMILE Affects Scheimpflug-based Dynamic Tonometry. *J Refract Surg*, 32(12), 821-828. <https://doi.org/10.3928/1081597X-20160816-02>
- Fontes, B. M., Ambrosio, R., Jr., Jardim, D., Velarde, G. C., & Nose, W. (2010). Corneal biomechanical metrics and anterior segment parameters in mild keratoconus. *Ophthalmology*, 117(4), 673-679. <https://doi.org/10.1016/j.ophtha.2009.09.023>
- Franco, J., White, C. A., & Kruh, J. N. (2020). Analysis of Compensatory Corneal Epithelial Thickness Changes in Keratoconus Using Corneal Tomography. *Cornea*, 39(3), 298-302. <https://doi.org/10.1097/ICO.0000000000002156>
- Gasset, A. R., Houde, W. L., & Garcia-Bengochea, M. (1978). Hard contact lens wear as an environmental risk in keratoconus. *Am J Ophthalmol*, 85(3), 339-341. [https://doi.org/10.1016/s0002-9394\(14\)77725-6](https://doi.org/10.1016/s0002-9394(14)77725-6)
- Godefrooij, D. A., de Wit, G. A., Uiterwaal, C. S., Imhof, S. M., & Wisse, R. P. (2017). Age-specific Incidence and Prevalence of Keratoconus: A Nationwide Registration Study. *Am J Ophthalmol*, 175, 169-172. <https://doi.org/10.1016/j.ajo.2016.12.015>

- Gomes, J. A., Rapuano, C. J., Belin, M. W., Ambrosio, R., Jr., Group of Panelists for the Global Delphi Panel of, K., & Ectatic, D. (2015). Global Consensus on Keratoconus Diagnosis. *Cornea*, 34(12), e38-39. <https://doi.org/10.1097/ICO.0000000000000623>
- Gonzalez, V., & McDonnell, P. J. (1992). Computer-assisted corneal topography in parents of patients with keratoconus. *Arch Ophthalmol*, 110(10), 1413-1414. <https://doi.org/10.1001/archophth.1992.01080220074024>
- Gordon-Shaag, A., Millodot, M., Shneur, E., & Liu, Y. (2015). The genetic and environmental factors for keratoconus. *Biomed Res Int*, 2015, 795738. <https://doi.org/10.1155/2015/795738>
- Greenstein, S. A., Fry, K. L., & Hersh, P. S. (2012). Effect of topographic cone location on outcomes of corneal collagen cross-linking for keratoconus and corneal ectasia. *J Refract Surg*, 28(6), 397-405. <https://doi.org/10.3928/1081597X-20120518-02>
- Hafezi, F., Kling, S., Gilardoni, F., Hafezi, N., Hillen, M., Abrishamchi, R., Gomes, J. A. P., Mazzotta, C., Randleman, J. B., & Torres-Netto, E. A. (2021). Individualized Corneal Cross-linking With Riboflavin and UV-A in Ultrathin Corneas: The Sub400 Protocol. *Am J Ophthalmol*, 224, 133-142. <https://doi.org/10.1016/j.ajo.2020.12.011>
- Henein, C., & Nanavaty, M. A. (2017). Systematic review comparing penetrating keratoplasty and deep anterior lamellar keratoplasty for management of keratoconus. *Cont Lens Anterior Eye*, 40(1), 3-14. <https://doi.org/10.1016/j.clae.2016.10.001>
- Hersh, P. S., Stulting, R. D., Muller, D., Durrie, D. S., Rajpal, R. K., & United States Crosslinking Study, G. (2017). United States Multicenter Clinical Trial of Corneal Collagen Crosslinking for Keratoconus Treatment. *Ophthalmology*, 124(9), 1259-1270. <https://doi.org/10.1016/j.ophtha.2017.03.052>
- Kaushik, S., & Pandav, S. S. (2012). Ocular Response Analyzer. *J Curr Glaucoma Pract*, 6(1), 17-19. <https://doi.org/10.5005/jp-journals-10008-1103>
- Kennedy, R. H., Bourne, W. M., & Dyer, J. A. (1986). A 48-year clinical and epidemiologic study of keratoconus. *Am J Ophthalmol*, 101(3), 267-273. [https://doi.org/10.1016/0002-9394\(86\)90817-2](https://doi.org/10.1016/0002-9394(86)90817-2)
- Krachmer, J. H., Feder, R. S., & Belin, M. W. (1984). Keratoconus and related noninflammatory corneal thinning disorders. *Surv Ophthalmol*, 28(4), 293-322. [https://doi.org/10.1016/0039-6257\(84\)90094-8](https://doi.org/10.1016/0039-6257(84)90094-8)
- Kreps, E. O., Claerhout, I., & Koppen, C. (2021). Diagnostic patterns in keratoconus. *Cont Lens Anterior Eye*, 44(3), 101333. <https://doi.org/10.1016/j.clae.2020.05.002>
- Labiris, G., Gatzioufas, Z., Sideroudi, H., Giarmoukakis, A., Kozobolis, V., & Seitz, B. (2013). Biomechanical diagnosis of keratoconus: evaluation of the keratoconus match index and the keratoconus match probability. *Acta Ophthalmol*, 91(4), e258-262. <https://doi.org/10.1111/aos.12056>
- Labiris, G., Giarmoukakis, A., Sideroudi, H., Song, X., Kozobolis, V., Seitz, B., & Gatzioufas, Z. (2014). Diagnostic capacity of biomechanical indices from a dynamic bidirectional applanation device in pellucid marginal degeneration. *J*

- Cataract Refract Surg*, 40(6), 1006-1012.
<https://doi.org/10.1016/j.jcrs.2014.03.018>
- Luce, D., & Taylor, D. . (2016). Ocular Response Analyzer In C. J. R. J. Liu (Ed.), *Corneal Biomechanics: From Theory to Practice*.
- Luz, A., Fontes, B. M., Lopes, B., Ramos, I., Schor, P., & Ambrosio, R., Jr. (2013). ORA waveform-derived biomechanical parameters to distinguish normal from keratoconic eyes. *Arq Bras Oftalmol*, 76(2), 111-117.
<https://doi.org/10.1590/s0004-27492013000200011>
- Mahmoud, A. M., Roberts, C. J., Lembach, R. G., Twa, M. D., Herderick, E. E., McMahon, T. T., & Group, C. S. (2008). CLMI: the cone location and magnitude index. *Cornea*, 27(4), 480-487. <https://doi.org/10.1097/ICO.0b013e31816485d3>
- Marcos, S. K. L. R. A. P.-E. J. M.-L. S. (2010). Corneal Biomechanical Changes after Collagen Cross-Linking from Porcine Eye Inflation Experiments. *Investigative Ophthalmology & Visual Science*, 51.
<https://doi.org/https://doi.org/10.1167/iovs.09-4536>
- Martin, R. (2018). Cornea and anterior eye assessment with placido-disc keratometry, slit scanning evaluation topography and scheimpflug imaging tomography. *Indian J Ophthalmol*, 66(3), 360-366. https://doi.org/10.4103/ijo.IJO_850_17
- Medeiros, F. A., Meira-Freitas, D., Lisboa, R., Kuang, T. M., Zangwill, L. M., & Weinreb, R. N. (2013). Corneal hysteresis as a risk factor for glaucoma progression: a prospective longitudinal study. *Ophthalmology*, 120(8), 1533-1540.
<https://doi.org/10.1016/j.ophtha.2013.01.032>
- Meek, K. M., Tuft, S. J., Huang, Y., Gill, P. S., Hayes, S., Newton, R. H., & Bron, A. J. (2005). Changes in collagen orientation and distribution in keratoconus corneas. *Invest Ophthalmol Vis Sci*, 46(6), 1948-1956. <https://doi.org/10.1167/iovs.04-1253>
- Mimouni, M., Sorkin, N., Trinh, T., Group, K. C. S., Hatch, W., & Singal, N. (2021). Central versus paracentral cone location and outcomes of accelerated cross-linking in keratoconus patients. *Eye (Lond)*, 35(12), 3311-3317.
<https://doi.org/10.1038/s41433-021-01404-5>
- Moshirfar, M., Motlagh, M. N., Murri, M. S., Momeni-Moghaddam, H., Ronquillo, Y. C., & Hoopes, P. C. (2019). Galilei Corneal Tomography for Screening of Refractive Surgery Candidates: A Review of the Literature, Part II. *Med Hypothesis Discov Innov Ophthalmol*, 8(3), 204-218.
<https://www.ncbi.nlm.nih.gov/pubmed/31598521>
- Moshirfar, M., Tukan, A. N., Bundogji, N., Liu, H. Y., McCabe, S. E., Ronquillo, Y. C., & Hoopes, P. C. (2021). Ectasia After Corneal Refractive Surgery: A Systematic Review. *Ophthalmol Ther*, 10(4), 753-776. <https://doi.org/10.1007/s40123-021-00383-w>
- Naderan, M., Jahanrad, A., & Farjadnia, M. (2018). Ocular, corneal, and internal aberrations in eyes with keratoconus, forme fruste keratoconus, and healthy eyes. *Int Ophthalmol*, 38(4), 1565-1573. <https://doi.org/10.1007/s10792-017-0620-5>
- Nicula CA, B. A., Nicula D, Nicula AP, Horvath KU and Bolboacă SD. (2022). Performances of Corneal Topography and Tomography in the Diagnosis of

- Subclinical and Clinical Keratoconus. *Front. Med.*, 9. <https://doi.org/doi:10.3389/fmed.2022.904604>
- Ortiz, D., Pinero, D., Shabayek, M. H., Arnalich-Montiel, F., & Alio, J. L. (2007). Corneal biomechanical properties in normal, post-laser in situ keratomileusis, and keratoconic eyes. *J Cataract Refract Surg*, 33(8), 1371-1375. <https://doi.org/10.1016/j.jcrs.2007.04.021>
- Perry, H. D., Buxton, J. N., & Fine, B. S. (1980). Round and oval cones in keratoconus. *Ophthalmology*, 87(9), 905-909. [https://doi.org/10.1016/s0161-6420\(80\)35145-2](https://doi.org/10.1016/s0161-6420(80)35145-2)
- Prevedel, R., Diz-Munoz, A., Ruocco, G., & Antonacci, G. (2019). Brillouin microscopy: an emerging tool for mechanobiology. *Nat Methods*, 16(10), 969-977. <https://doi.org/10.1038/s41592-019-0543-3>
- Qin, X., Yu, M., Zhang, H., Chen, X., & Li, L. (2019). The Mechanical Interpretation of Ocular Response Analyzer Parameters. *Biomed Res Int*, 2019, 5701236. <https://doi.org/10.1155/2019/5701236>
- Rabinowitz, Y. S. (1998). Keratoconus. *Surv Ophthalmol*, 42(4), 297-319. [https://doi.org/10.1016/s0039-6257\(97\)00119-7](https://doi.org/10.1016/s0039-6257(97)00119-7)
- Randleman, J. B., Khandelwal, S. S., & Hafezi, F. (2015). Corneal cross-linking. *Surv Ophthalmol*, 60(6), 509-523. <https://doi.org/10.1016/j.survophthal.2015.04.002>
- Roberts, C. J., & Dupps, W. J., Jr. (2014). Biomechanics of corneal ectasia and biomechanical treatments. *J Cataract Refract Surg*, 40(6), 991-998. <https://doi.org/10.1016/j.jcrs.2014.04.013>
- Romero-Jimenez, M., Santodomingo-Rubido, J., & Wolffsohn, J. S. (2010). Keratoconus: a review. *Cont Lens Anterior Eye*, 33(4), 157-166; quiz 205. <https://doi.org/10.1016/j.clae.2010.04.006>
- Santodomingo-Rubido, J., Carracedo, G., Suzaki, A., Villa-Collar, C., Vincent, S. J., & Wolffsohn, J. S. (2022). Keratoconus: An updated review. *Cont Lens Anterior Eye*, 45(3), 101559. <https://doi.org/10.1016/j.clae.2021.101559>
- Scarcelli, G., Besner, S., Pineda, R., Kalout, P., & Yun, S. H. (2015). In vivo biomechanical mapping of normal and keratoconus corneas. *JAMA Ophthalmol*, 133(4), 480-482. <https://doi.org/10.1001/jamaophthalmol.2014.5641>
- Scarcelli, G., Besner, S., Pineda, R., & Yun, S. H. (2014). Biomechanical characterization of keratoconus corneas ex vivo with Brillouin microscopy. *Invest Ophthalmol Vis Sci*, 55(7), 4490-4495. <https://doi.org/10.1167/iovs.14-14450>
- Sedaghat, M. R., Momeni-Moghaddam, H., Azimi Khorasani, A., Belin, M. W., Monfared, N., Wolffsohn, J. S., Pakdel, M., Farrokh Ghate, M., & Hemmatian, Z. (2021). Comparison of Keratoconus Cone Location of Different Topo/tomographical Parameters. *Curr Eye Res*, 46(11), 1666-1672. <https://doi.org/10.1080/02713683.2021.1931343>
- Shah, S., & Laiquzzaman, M. (2009). Comparison of corneal biomechanics in pre and post-refractive surgery and keratoconic eyes by Ocular Response Analyser. *Cont Lens Anterior Eye*, 32(3), 129-132; quiz 151. <https://doi.org/10.1016/j.clae.2008.12.009>
- Shah, S., Laiquzzaman, M., Bhojwani, R., Mantry, S., & Cunliffe, I. (2007). Assessment of the biomechanical properties of the cornea with the ocular response analyzer in

- normal and keratoconic eyes. *Invest Ophthalmol Vis Sci*, 48(7), 3026-3031. <https://doi.org/10.1167/iovs.04-0694>
- Shao, P., Eltony, A. M., Seiler, T. G., Tavakol, B., Pineda, R., Koller, T., Seiler, T., & Yun, S. H. (2019). Spatially-resolved Brillouin spectroscopy reveals biomechanical abnormalities in mild to advanced keratoconus in vivo. *Sci Rep*, 9(1), 7467. <https://doi.org/10.1038/s41598-019-43811-5>
- Shetty, R., Nuijts, R. M., Nicholson, M., Sargod, K., Jayadev, C., Veluri, H., & Sinha Roy, A. (2015). Cone location-dependent outcomes after combined topography-guided photorefractive keratectomy and collagen cross-linking. *Am J Ophthalmol*, 159(3), 419-425 e412. <https://doi.org/10.1016/j.ajo.2014.11.020>
- Steinwender, G., Kollenc, A., Shajari, M., Sommer, M., Borenich, A., Horwath-Winter, J., Lindner, E., Woltsche, N., List, W., & Wedrich, A. (2022). Determining the center of a keratoconus: Comparison of different tomographic parameters and impact of disease severity. *Front Med (Lausanne)*, 9, 968318. <https://doi.org/10.3389/fmed.2022.968318>
- Susanna, C. N., Diniz-Filho, A., Daga, F. B., Susanna, B. N., Zhu, F., Ogata, N. G., & Medeiros, F. A. (2018). A Prospective Longitudinal Study to Investigate Corneal Hysteresis as a Risk Factor for Predicting Development of Glaucoma. *Am J Ophthalmol*, 187, 148-152. <https://doi.org/10.1016/j.ajo.2017.12.018>
- Taroni, L., Bernabei, F., Pellegrini, M., Roda, M., Toschi, P. G., Mahmoud, A. M., Schiavi, C., Giannaccare, G., & Roberts, C. J. (2020). Corneal Biomechanical Response Alteration After Scleral Buckling Surgery for Rhegmatogenous Retinal Detachment. *Am J Ophthalmol*, 217, 49-54. <https://doi.org/10.1016/j.ajo.2020.03.054>
- Tian, L., Huang, Y. F., Wang, L. Q., Bai, H., Wang, Q., Jiang, J. J., Wu, Y., & Gao, M. (2014). Corneal biomechanical assessment using corneal visualization scheimpflug technology in keratoconic and normal eyes. *J Ophthalmol*, 2014, 147516. <https://doi.org/10.1155/2014/147516>
- Vinciguerra, R., Ambrosio, R., Jr., Elsheikh, A., Roberts, C. J., Lopes, B., Morenghi, E., Azzolini, C., & Vinciguerra, P. (2016). Detection of Keratoconus With a New Biomechanical Index. *J Refract Surg*, 32(12), 803-810. <https://doi.org/10.3928/1081597X-20160629-01>
- Wang, Y., Rabinowitz, Y. S., Rotter, J. I., & Yang, H. (2000). Genetic epidemiological study of keratoconus: evidence for major gene determination. *Am J Med Genet*, 93(5), 403-409. <https://www.ncbi.nlm.nih.gov/pubmed/10951465>
- Wells, A. P., Garway-Heath, D. F., Poostchi, A., Wong, T., Chan, K. C., & Sachdev, N. (2008). Corneal hysteresis but not corneal thickness correlates with optic nerve surface compliance in glaucoma patients. *Invest Ophthalmol Vis Sci*, 49(8), 3262-3268. <https://doi.org/10.1167/iovs.07-1556>
- Wilson, S. E., He, Y. G., Weng, J., Li, Q., McDowall, A. W., Vital, M., & Chwang, E. L. (1996). Epithelial injury induces keratocyte apoptosis: hypothesized role for the interleukin-1 system in the modulation of corneal tissue organization and wound healing. *Exp Eye Res*, 62(4), 325-327. <https://doi.org/10.1006/exer.1996.0038>
- Wojcik, K. A., Kaminska, A., Blasiak, J., Szaflik, J., & Szaflik, J. P. (2013). Oxidative stress in the pathogenesis of keratoconus and Fuchs endothelial corneal

- dystrophy. *Int J Mol Sci*, 14(9), 19294-19308.
<https://doi.org/10.3390/ijms140919294>
- Yang, K., Xu, L., Fan, Q., Zhao, D., & Ren, S. (2019). Repeatability and comparison of new Corvis ST parameters in normal and keratoconus eyes. *Sci Rep*, 9(1), 15379.
<https://doi.org/10.1038/s41598-019-51502-4>
- Yuhas, P. T., & Roberts, C. J. (2023). Clinical Ocular Biomechanics: Where Are We after 20 Years of Progress? *Curr Eye Res*, 48(2), 89-104.
<https://doi.org/10.1080/02713683.2022.2125530>
- Zadnik, K., Steger-May, K., Fink, B. A., Joslin, C. E., Nichols, J. J., Rosenstiel, C. E., Tyler, J. A., Yu, J. A., Raasch, T. W., Schechtman, K. B., & Keratoconus, C. S. G. C. L. E. o. (2002). Between-eye asymmetry in keratoconus. *Cornea*, 21(7), 671-679. <https://doi.org/10.1097/00003226-200210000-00008>
- Zhang, X., Munir, S. Z., Sami Karim, S. A., & Munir, W. M. (2021). A review of imaging modalities for detecting early keratoconus. *Eye (Lond)*, 35(1), 173-187.
<https://doi.org/10.1038/s41433-020-1039-1>
- Yuhas, P. T., & Roberts, C. J. (2023). Clinical Ocular Biomechanics: Where Are We after 20 Years of Progress? *Curr Eye Res*, 48(2), 89-104.
<https://doi.org/10.1080/02713683.2022.2125530>
- Zadnik, K., Steger-May, K., Fink, B. A., Joslin, C. E., Nichols, J. J., Rosenstiel, C. E., Tyler, J. A., Yu, J. A., Raasch, T. W., Schechtman, K. B., & Keratoconus, C. S. G. C. L. E. o. (2002). Between-eye asymmetry in keratoconus. *Cornea*, 21(7), 671-679. <https://doi.org/10.1097/00003226-200210000-00008>
- Zhang, X., Munir, S. Z., Sami Karim, S. A., & Munir, W. M. (2021). A review of imaging modalities for detecting early keratoconus. *Eye (Lond)*, 35(1), 173-187.
<https://doi.org/10.1038/s41433-020-1039-1>

Appendix A

Measurement-type agreement for IOP and biomechanical parameters in the case cohort (n = 78 eyes) and control cohort (n = 144 eyes). Bland-Altman plots for (A) corneal-compensated IOP (IOP_{cc}), (B) Goldmann-correlated IOP (IOP_g), (C) corneal hysteresis (CH), (D) waveform score (WS), (E) area under first applanation peak (p1area), (F) area under second applanation peak (p2area), (G) height of first applanation peak (h1), (H) height of second applanation peak (h2), (I) width of first applanation peak (w1), (J) width of second applanation peak (w2), and (K) Keratoconus Match Index (KMI). The blue circles represent case subjects, and the red circles represent control subjects. Solid black lines are the mean for each cohort, and the red dashed lines are the 95% limits of agreement for each cohort.

